J. Fluid Mech. (1999), *vol.* 391, *pp.* 91–122. Printed in the United Kingdom

Examination of large-scale structures in a turbulent plane mixing layer. Part 1. Proper orthogonal decomposition

By J. DELVILLE[1], L. UKEILEY[2]†, L. CORDIER[1], J. P. BONNET[1] AND M. GLAUSER[2]

[1]LEA/CEAT UMR CNRS 6609, Université de Poitiers, 43 route de l'Aérodrome, F-86036 Poitiers, France

[2]Clarkson University, Potsdam, NY 13699-5725, USA

(Received 24 March 1998 and in revised form 6 January 1999)

Large-scale structures in a plane turbulent mixing layer are studied through the use of the proper orthogonal decomposition (POD). Extensive experimental measurements are obtained in a turbulent plane mixing layer by means of two cross-wire rakes aligned normal to the direction of the mean shear and perpendicular to the mean flow direction. The measurements are acquired well into the asymptotic region. From the measured velocities the two-point spectral tensor is calculated as a function of separation in the cross-stream direction and spanwise and streamwise wavenumbers. The continuity equation is then used for the calculation of the non-measured components of the tensor. The POD is applied using the cross-spectral tensor as its kernel. This decomposition yields an optimal basis set in the mean square sense. The energy contained in the POD modes converges rapidly with the first mode being dominant (49% of the turbulent kinetic energy). Examination of these modes shows that the first mode contains evidence of both known flow organizations in the mixing layer, i.e. quasi-two-dimensional spanwise structures and streamwise aligned vortices. Using the shot-noise theory the dominant mode of the POD is transformed back into physical space. This structure is also indicative of the known flow organizations.

1. Introduction

The existence of large-scale coherent motions in turbulent flows has been under investigation for several decades. During this time, several definitions as well as a multitude of techniques have been developed to identify them. These involve statistical means, instantaneous flow patterns (pseudo and direct), stability theory, topological methods, conditional techniques and those developed from dynamical systems theory. However different they are, there seems to be a general consensus that a definition and means of identifying coherent structures are necessary for understanding and predicting turbulence. Another consensus in coherent structure research is the need to study the three-dimensionality and dynamics of these structures. In that vein, this work appears to be the first to study the three-dimensionality and dynamics of the large-scale structures in the plane turbulent mixing layer simultaneously through the use of the proper orthogonal decomposition (POD).

† Present address: National Research Council, NASA Langley Research Center, Mail Stop 166, Hampton, VA 23681, USA.

1.1. *Large-scale structures in turbulent mixing layers*

It is now well known that two main flow organizations co-exist in mixing layers: a quasi-two-dimensional spanwise aligned vortex tube with streamwise aligned vortices imposed on them. It has been proposed by Pierrehumbert & Widnall (1982) that the same flow phenomena (i.e. pairing, amalgamation, tearing, etc.) govern the turbulent mixing layer as well as its laminar counterpart. The visualizations of Brown & Roshko (1974) are widely recognized as being the first to identify the large-scale spanwise vortex structure in the plane mixing layer, while Konrad (1976) and Breidenthal (1978) showed the first strong visual evidence of the streamwise aligned vortices. Several theories based on instabilities, such as Kelvin–Helmholtz instability, have been developed to explain the formation and evolution of the primary (spanwise) and secondary (streamwise) vortical structures and are described in reviews by Ho & Huerre (1984) and Liu (1989).

The visualization studies were continued by Bernal & Roshko (1986) with an emphasis on the streamwise aligned vorticity. In particular they studied their origin, interaction with the spanwise vorticity and their role in the development of the mixing layer. It was found that the average spacing of the streamwise structures was 0.67 when normalized by the local mean spacing of the spanwise vortices and it was independent of velocity ratio. It was also shown that the smaller-scale secondary structures embedded in the spanwise rollers did not destroy their 'coherence'. Summaries of findings from several flow visualization experiments are found in a review by Browand (1986). In this review it was suggested that the large-scale motions behave as a dynamical system with relatively few degrees of freedom. This author further speculated that the turbulent mixing layer exhibits chaotic behaviour in both space and time. This appears to be the first suggestion that a dynamical system model, as reported in Part 2 of the current study (Ukeiley *et al.* 1999), may prove fruitful in the turbulent mixing layer.

Since the early flow visualization work, many other experimental studies of mixing layers have been conducted to study the existence and origins of the vortical structures. In a series of studies, Lasheras & Choi (1988), Meiburg & Lasheras (1988) and Lasheras & Meiburg (1990) explored the initial conditions triggering the instabilities that generate the streamwise aligned structures. The shear layer examined was generated by a flat plate with a small-amplitude sinusoidal perturbation in the spanwise direction to enhance the streamwise vortices for easier study. Some of their conclusions are: vortex tubes were formed from the stretching of weak perturbed vorticity in the braids of the Kármán vortices; redistribution, reorientation and stretching of the spanwise vorticity led to counter-rotating pairs of three-dimensional streamwise vortex tubes; and this vorticity exists in an array of closed vortex loops with alternating signs appearing in a staggered configuration.

In another series of studies initiated in Bell & Mehta (1992) and continued in Leboeuf & Mehta (1993), an attempt was made to 'quantitatively' establish the presence and role of the secondary vortical structures in the mixing layer. They postulated that the streamwise structure originated from streamwise vortices in the upstream boundary layer. They found the circulation of the streamwise vortices to be 10% of that of the spanwise vortices. Also, they found that the vortices initially appeared in groups of three, then unwrapped to form a row of alternating-sign streamwise vortices consistent with the findings of Meiburg & Lasheras (1988). They showed evidence of the streamwise vortices in the self-similar region although their

strength was decaying. It was concluded that one of the major effects of the streamwise vortices was to produce higher Reynolds stress values.

Direct numerical simulations were used by Metcalfe *et al*. (1987) to study the three-dimensional stability of two-dimensional vortical states. They found that forcing of wavenumbers associated with pairing could keep the flow two-dimensional. They also showed that the flow would reach a state with high levels of vorticity in the braids if the pairing mode was the primary mode of forcing. It was also noted that for three-dimensional simulations, streamwise aligned pairs of counter-rotating vortices appeared even in the absence of pairing mode excitation. Their major conclusions were that small-scale three-dimensional disturbances transform themselves into streamwise vorticity, and there is evidence of the three-dimensionality of the flow in the spanwise vortex cores.

Moser & Rogers (1992) studied a temporally evolving simulated turbulent mixing layer for evidence of coherent structures. They found that in the self-similar (asymptotic) region there is a fundamental difference in the coherent structures found from those in the transitional region or the laminar counterpart. They observed that in this region there were neither pairings nor rib vortices. Their results showed that the turbulence in the braid region is qualitatively the same as that in the roller. These results strongly disagree with the findings of the flow visualization results. They postulated that the experiments have stronger two-dimensional disturbances such as those that would arise from the receptivity of the splitter plate tip. Their findings show that a model for the mixing layer should not be based on the quasi-two-dimensional structure since their only dynamical significance appears to be that they create a strain and rotation-dominated regions and not the growth rate of the mixing layer.

1.2. *Proper orthogonal decomposition*

Lumley proposed the POD technique to objectively identify the coherent structure or 'dominant eddy' in a turbulent flow. The method was first applied to the wake behind a cylinder by Payne (1966). The results of this study showed that the energy content in the dominant eddy was not significantly larger than that in subsequent eddies. Bakewell & Lumley (1967) applied the technique to measurements taken in the near-wall region of turbulent pipe flow. These results were more conclusive, showing the dominant eddy to contain 90% of the total streamwise turbulent energy.

Following the original work of Lumley and coworkers, two relatively recent events have lead to more studies utilizing POD. They are the advancement of computer simulations and the development of more advanced data acquisition techniques. Comprehensive reviews of applications of the POD can be found in Berkooz, Holmes & Lumley (1993) and Delville (1995). Some of the findings for applications to turbulent flows and extensions to the theory are detailed below.

The POD has been applied to most imaginable flow configurations. The earliest applications of the POD in the turbulent boundary layer were by Moin (1984), Herzog (1986) and Moin & Moser (1989). Their results all showed a dominant mode containing up to 64% of the turbulent kinetic energy. Moin & Moser (1989) were able to experiment with the domain over which they applied the POD, showing the importance of spanning a relevant area. In the first application of the POD to free shear flows Leib, Glauser & George (1984), Glauser, Leib & George (1987) and Glauser & George (1987) applied the POD to the near-field region of a turbulent axisymmetric jet, showing that the dominant eigenmode contained approximately 40% of the total turbulent kinetic energy. The complex flow field downstream of a lobed mixer was studied by Ukeiley *et al*. (1992) and Ukeiley, Glauser & Wick

(1993). In these studies the breakdown of the large-scale structure was tracked between downstream locations. Manhart & Wengle (1993) applied the space-time-symmetric fully three-dimensional version of the POD (not using Fourier modes in any direction) to a large-eddy simulation of turbulent flow over a surface-mounted cube. Rajaee, Karlsson & Sirovich (1994) applied the POD to measurements obtained in a forced mixing layer, showing the dominant spanwise vortex which was excited by their forcing.

The precursor to this work were extensive studies of applying the POD to data collected in a plane mixing layer, conducted by Delville *et al*. (1993). In the initial study using the POD, Delville, Bellin & Bonnet (1989) used data collected with a rake of 21 single-component hot wires, placed perpendicularly to the plate. They found that 70% of the mean-square streamwise velocity was recovered within the first three modes. In this study a pseudo flow visualization technique (see Delville *et al*. 1988) was also utilized to examine the contribution of the higher POD modes. Delville (1994) compared applications of various levels of the POD, i.e. scalar and vectorial. One finding was that, with higher degrees of complexity included in the kernel of the POD equation, more essential flow physics was contained in the first POD mode. He also postulated a scaling law and experimentally verified the Nyquist criteria for the POD modes postulated by Glauser & George (1992).

One of the limitations of the POD approach is due to the notion of loss of phase. When homogeneous directions are present within the flow, Fourier transforms are used in these directions, leading to a globally non-local description of the POD modes in physical space. Lumley (1981), Herzog (1986), Moin & Moser (1989) and Arndt, Long & Glauser (1997) used a complementary technique 'the shot-noise theory' in order to gain a description of the so-called 'dominant structure' in physical space.

Adaptations to the definition of the integral eigenvalue problem of the POD have also flourished in recent years. Sirovich (1987) proposed the method of snapshots as a numerical procedure which saves computational time for calculating the POD modes. This method uses the correlation of instantaneous snapshots of the flow. This reduces the order of the eigenvalue problem to that of the number of snapshots and not the physical mesh. Glezer, Kadioglu & Pearlstein (1989) developed an extension to the POD capable of dealing with flows in which long-term correlation measurements are not possible. This extended POD was applied to a time-periodically forced plane mixing layer and showed that as much as 78% of the information, collected from a rake of 10 wires placed in a cross-stream orientation, was recovered with a three-mode reconstruction. A technique which utilizes the linear stochastic estimation (LSE) to extend the instantaneous velocity field for the POD was reported by Ukeiley, Cole & Glauser (1993) and Bonnet *et al*. (1994). This technique utilizes the LSE to estimate the instantaneous velocity at all positions of interest and then projects the estimated velocity onto the eigenfunctions of the POD. This technique can be of great interest to experimentalists because it allows the study of the time evolution of the POD modes without having *a priori* knowledge of the full instantaneous flow field simultaneously. A similar approach has been used by Faghani (1997) in a turbulent plane jet configuration.

In studies to determine the universality of the POD eigenfunctions, Chambers *et al*. (1988) applied the POD to a randomly forced solution of Burgers' equation. Although this application was not in a turbulent flow, the solutions to Burgers' equation exhibit turbulent flow characteristics, i.e. small viscous scales near the boundaries and large outer scales. They found that the eigenfunctions in the core region were independent of Reynolds number, while the bandwidth of the eigenvalue spectra increased with it.

Following up this study, Liu, Adrian & Hanratty (1995) examined the eigenfunctions' dependence on Reynolds number for channel flow. They found, at least for the cases studied, that the eigenfunctions can be scaled to be applied at different Reynolds numbers.

The spatio-temporal behaviour of three-dimensional coherent structures in a transitional spatially evolving boundary layer was studied by Rempfer & Fasel (1994). They describe the dynamical coherent structures as pairs of eigenfunctions that contain complete information on the spatial evolution. Their findings showed that the first-order structures agreed well with structures observed in experiments. They were also able to link the higher-order POD structures to the spike-like signals observed in transitional regions.

1.3. *Present study*

This study can be broken down into several steps. The first step involves acquiring and manipulating the experimental data. The data are obtained in a plane mixing layer utilizing rakes of 'X' type hot wires, as described in § 2 and the cross-spectral tensor is calculated. The procedures for this phase are outlined in § 3. The second step applies the POD using the cross-spectral tensor from the first phase. This was done by first utilizing the cross-spectral tensor for streamwise and cross-stream velocities (§ 4), then using the full cross-spectral tensor for all three velocity components (§ 5). To do this, the continuity equation and Taylor's hypothesis are used to map the frequency dependence of the two-point spectral tensor to streamwise wavenumbers. The next step, as discussed in § 6, involves examining the dominant mode in physical space by using a 'shot-noise' decomposition. This allows a quantitative analysis of the large scales and a visual representation of their interactions in the flow. The final step, to be discussed in Part 2 of this paper, utilizes the eigenfunctions from step 2 as a basis set to develop a low-dimensional dynamical system model for the mixing layer. This is achieved by using the eigenfunctions from the POD in a Galerkin projection to yield a set of ordinary differential equations (ODE) for each streamwise/spanwise wavenumber pair kept in a given truncation (see Holmes, Lumley & Berkooz 1996). Several versions of the model are presented in Part 2 for severely truncated systems. The temporal dynamics are then studied through spectra, time histories of the projection coefficients of the POD modes and velocity vector plots.

2. Experiments

The data used for this study were acquired experimentally in the fully developed region of a two-stream plane mixing layer. The wind tunnel used in this study was a standard open loop facility designed for subsonic flows. The flow commences at an inlet box then flows into two streams through two different head loss devices which are followed by fine mesh screens. It then contracts down as it enters the test section. Next, the flow goes through a diffuser, then crosses the fan and finally exits through the silencer. A schematic of the facility is shown in figure 1.

The coordinate system chosen has x_1 (or x) as the streamwise, x_2 (or y) as the cross-stream and x_3 (or z) as the spanwise direction. The zeros are taken to be at the trailing edge of the splitter plate for x and the centre of the test section for both y and z, respectively. The test section is rectangular with dimensions of $30\times30\times120$ cm. The mixing layer is created by a steel flat plate splitting the streams. The velocity ratio between the streams ($U_a = 41.7$ and $U_b = 22.5$ m s^{-1}) is 0.59

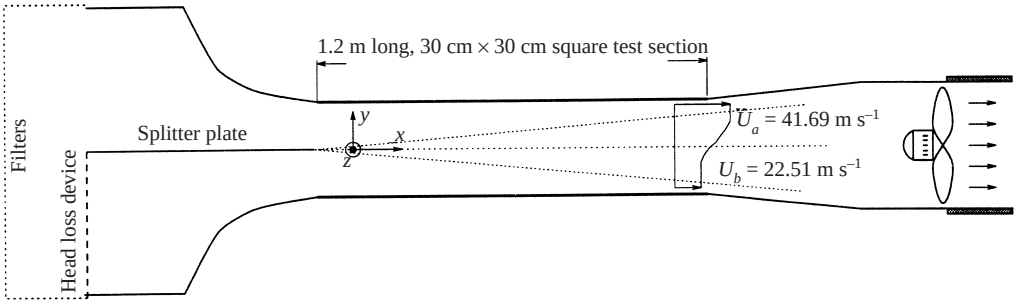

FIGURE 1. Schematic of wind tunnel.

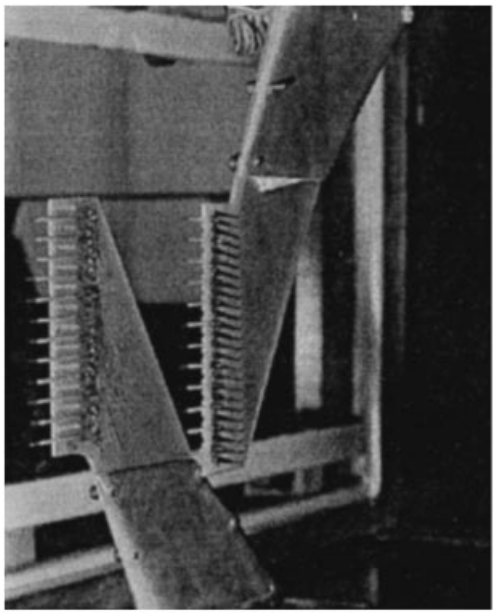

FIGURE 2. Placement of rakes in the wind tunnel.

with an average convective velocity $U_m = (U_a + U_b)/2$ of about 34 m s^{-1}. For more details on the facility the reader can refer to Bellin (1991). The external levels of turbulence are less than 0.3%. The boundary layers on the flat plate are fully turbulent with a momentum thickness $\theta \simeq 1$ mm. Previous studies have shown that at the streamwise location where the measurements were taken, 600 mm downstream of the splitting plate, the similarity state was obtained for the mean velocity profiles with an expansion factor σ being of the order of 43. At this location, the vorticity thickness δ_ω was of the order of 27.6 mm. The passage of the quasi-two-dimensional large-scale structure, monitored at the edge of the mixing layer ($y/\delta_\omega \simeq 0.5$) is characterized by a typical frequency f_p that leads to a typical Strouhal number $S_\omega = f_p \delta_\omega / U_m$ of order 0.3.

The velocity time series data were acquired through the use of two 'rakes' of hot-wire probes. Each array contained 12 probes in an 'X' configuration spaced by $\Delta_y =$ 6 mm (i.e. $\simeq \delta_\omega/4.6$). The rakes were aligned with the plate along the normal direction and spanned from approximately $-0.5\,L_y$ to $+0.5\,L_y$, where $L_y \simeq 3\,\delta_\omega$,

with no probes being truly at the centre. Figure 2 shows the placement of the two rakes in the facility. Two separate experiments were performed: the probes were first orientated to measure the u and v components of velocity (hereafter denoted the UV-experiment), then reorientated to measure u and w components of velocity (the UW-experiment). The experiments were conducted in an identical fashion, with one rake at the same fixed spanwise location and the other traversed through 32 equally spaced spanwise separations. The separation step, Δ_z, was 4.2 mm which is of the order of the Taylor micro-scale. The total distance spanned in the z direction was $L_z = 135$ mm which is approximately 5 times the local vorticity thickness. In each of the experiments, eight identical independent runs were performed, where the data were collected with the moving rake traversing through the 32 spanwise locations. In the UV-experiment, 16 runs were conducted; however, it was determined that the statistics did not vary significantly if only eight runs were utilized. For each separation of every run, seven sets of 10 240 data points per velocity component were taken. The 10 240 data points were then split into blocks of 1024 points. This technique yielded $8\times7\times10$ independent blocks which is the number of samples used in all the time averages. The total amount of data collected for each experiment was approximately 3.3 Giga Bytes.

The rakes and probes were constructed at the CEAT; specifications and dimensions can be found in Bellin (1991) and Delville (1995). Briefly, the probes are moulded out of an epoxy with broaches inserted in them to support the sensing wire. The actual sensing wire is tungsten with a diameter of 2.5 μm and a sensing length of approximately 0.5 mm. This yields an l/d ratio of 200. The rakes were made from an etched circuit board with grooved slots where the probes are soldered into place. By using probes in an 'X' configuration one can obtain two velocity components simultaneously in the plane defined by the sensing wires. Each of the wires, numbered n_i, will essentially resolve the component of velocity normal to its direction (u_{ni}). It is necessary to take into account the actual orientation of the wires to the mean flow. The law utilized in this study for taking implicitly this into account is similar to that of Collis and Williams, as presented in Bruun (1995), and is written for each wire i as follows:

$$e_i^2(T_{wi} - T_f) = \mathscr{A}_i(\alpha) + \mathscr{B}_i(\alpha)u_{ni}^{\mathscr{N}_i}, \tag{2.1}$$

where e_i is the voltage, T_{wi} is the temperature of the wire, T_f is the temperature of the flow, and $\mathscr{A}_i(\alpha)$ and $\mathscr{B}_i(\alpha)$ are fourth-order polynomials in α, where α is the direction of the flow relative to the probes. The rakes of probes were calibrated in a separate rectangular jet facility with a very low core turbulence intensity. The rakes are traversed over nine angles from $+30^\circ$ to -30° with velocities ranging from 20 to 50 m s^{-1} and temperature variations. This technique leads to a system of equations for (2.1), which is then solved through an iterative least-squares matrix method.

A set of 48 constant temperature anemometers (CTA T.S.I. 1750) drove the hot wires. The temporal averaged (1 Hz low-pass filtered) and the fluctuating parts (1 Hz high-pass filtered) arising from the anemometers were, after proper amplification, acquired independently (12 bits ADC). For all of the experiments performed, signals were simultaneously sampled at a sampling frequency f_s=10 kHz and low-pass filtered at 5 kHz. As stated above the fluctuating data were broken into blocks of 1024 samples. This leads to a frequency resolution of approximately 10 Hz and a total time for each block of 0.1 s which contains approximately 40 structures based on the characteristic Strouhal number of the mixing layer measured at the streamwise location where experiments were performed.

3. Spectral and correlation tensors

From the experimentally measured data the cross-spectral tensor ($\Psi_{ij}(y, y'; f, k_z)$, that is the direct double Fourier transform of the correlation tensor $R_{ij}(y, y'; \tau, \delta_z) = \langle u_i(y, z, t) u_j(y', z+\delta_z, t+\tau) \rangle$) is calculated in a two-step process, by applying a spanwise Fourier transform of the quasi-spectral tensor $S_{ij}(y, y'; f, \delta_z)$.

3.1. *Calculation*

In the first step the quasi-spectral tensor $S_{ij}(y, y'; f, \delta_z)$ was calculated as a function of frequency f and for each spanwise separation δ_z. This was done by first applying a direct time-to-frequency Fourier transform to all of the measured records of velocity as follows:

$$\tilde{u}_i(y, z; f) = \int_{-\infty}^{\infty} u_i(y, z, t) \mathrm{e}^{-\mathrm{i}2\pi f t} \mathrm{d}t, \tag{3.1}$$

where $i = 1$ and 2 for the first UV-experiment and $i = 1$ and 3 for the second UW-experiment, i denotes $(-1)^{1/2}$, f is frequency and t is time. The spectral tensor was then calculated from the following equation:

$$S_{ij}(y, y'; f, \delta_z) = \langle \tilde{u}_i^*(y, z = 0; f) \tilde{u}_j(y', z = \delta_z; f) \rangle, \tag{3.2}$$

where $\langle\ \rangle$ represents a 'block' ensemble average and * denotes the complex conjugate. As stated previously a block size of 1024 points with 560 independent blocks was used for the average. These values were then smoothed using a 10% bandwidth moving filter.

The next step involved applying a Fourier transform over the spanwise direction to obtain the cross-spectral tensor as a function of k_z. The amount of data collection was reduced by a factor of nearly two because the spanwise direction was assumed to be homogeneous and symmetric. This means that only positive separations, in z, were measured and the negative separations were mapped by the following symmetry:

$$S_{ij}(y, y'; f, \delta_z) = \pm S_{ij}(y, y'; f, -\delta_z), \tag{3.3}$$

where the minus is for i or j equal to 3 but not for both. Once the mapping to negative separations in z was performed, a Fourier transform was applied over the spanwise data for each frequency and (y, y') pair. This Fourier transform can be represented by the following equation:

$$\Psi_{ij}(y, y'; f, k_z) = \int_{-\infty}^{\infty} S_{ij}(y, y'; f, \delta_z) \mathrm{e}^{-\mathrm{i}2\pi k_z \delta_z} \mathrm{d}\delta_z. \tag{3.4}$$

A weighting function $\gamma(\delta_z)$ was introduced in (3.4) in order to take into account the effects due to the limited extent of experiments in the spanwise direction, and γS_{ij} was Fourier transformed instead of S_{ij}. The Gaussian window function $\gamma(\delta_z) = 1.84\mathrm{e}^{-(3\delta_z/L_z)^2/2}$ was used. After the application of the Fourier transform, the data were smoothed in the k_z-direction using a 20% bandwidth moving filter. In order to examine the effect of spatial aliasing as discussed by Glauser & George (1992), the calculation of $\Psi_{ij}(y, y'; f, k_z)$ was also performed with only 16 points to represent the same spatial extent L_z (i.e. while doubling Δ_z). It was found that there were no significant differences in the spectral tensor.

3.2. *Analysis*

It is of interest to examine the correlation and spectral tensors of the original data to get an idea of the integral scales and energy distribution. These quantities will become

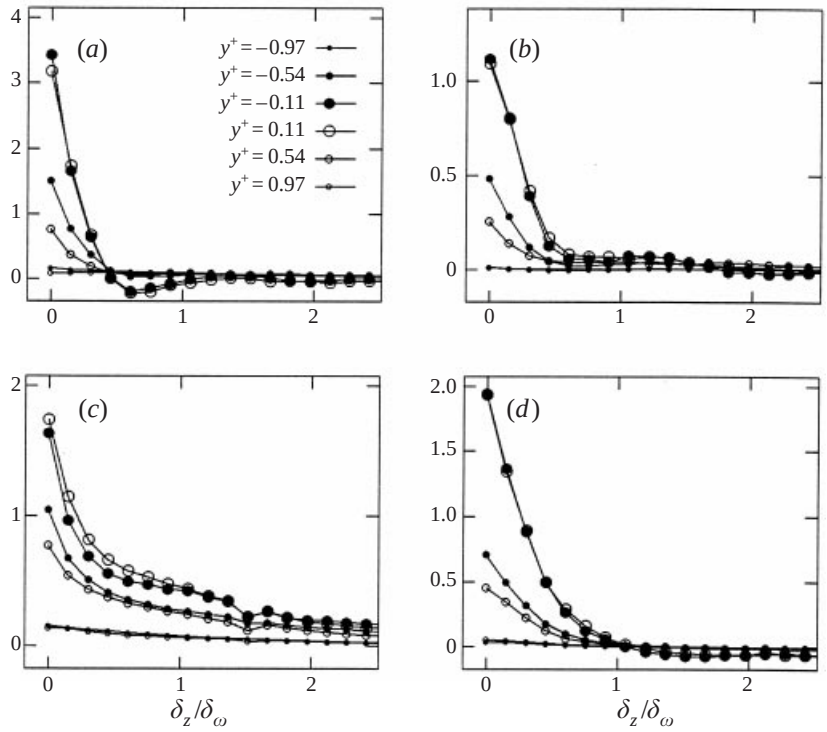

FIGURE 3. Spanwise correlations for some selected $y^+ = y/\delta_\omega$ locations. Plotted are $100 \times R_{ij}(y^+, y^+; \delta_z, \tau{=}0)/\Delta U^2$: (*a*) R_{11}, (*b*) $-R_{12}$, (*c*) R_{22}, (*d*) R_{33}.

important when a truncation is defined for the POD-based dynamical systems model discussed in Part 2 of this paper. At this stage, the spectra Ψ_{ij} are known for ij=11, 12, 22, 33 and 13. The five cross-spectra are described for 512 discrete frequencies, over 12×12 (y, y') positions and for 32 spanwise wavenumbers k_z. We will limit the present analysis to a few significant correlations, by considering only configurations where $y = y'$. This analysis is performed either in physical space, i.e. space–time correlations, or in Fourier space, i.e. cross-spectra.

3.2.1. *Correlation tensor*

Figures 3(*a*) to 3(*d*) show the correlation tensor $R_{ij}(y, y; \delta_z, \tau)$ as a function of δ_z. The correlations are normalized by the mean streamwise velocity difference $\Delta U = U_a - U_b$. The spanwise correlations are obtained by inverse Fourier transforming S_{ij} (in the time direction) and only considering $\tau = 0$. These correlations are plotted for some selected y^+ locations within the mixing layer (where $y^+ = y/\delta_\omega$). Among the 12 y^+ positions available, only six, symmetrically located relatively to the mixing layer axis, are shown: two of them are in the external zone of the mixing layer ($|y^+| \simeq 1$), two of them are close to the mixing layer edge ($|y^+| \simeq 0.5$), and the last two lie near the mixing layer axis ($|y^+| \simeq 0.1$). Whatever the plot, a strong symmetry of the correlation tensor, relative to the mixing layer axis, can be noticed.

In the outer region of the mixing layer, one should note that the correlation remains fairly constant in z. The level of the correlation remains low, but it should be recalled that R_{ij} is not a correlation coefficient, because ΔU is used for normalization. This can be interpreted as the correlations in the outer region highlighting the quasi-two-

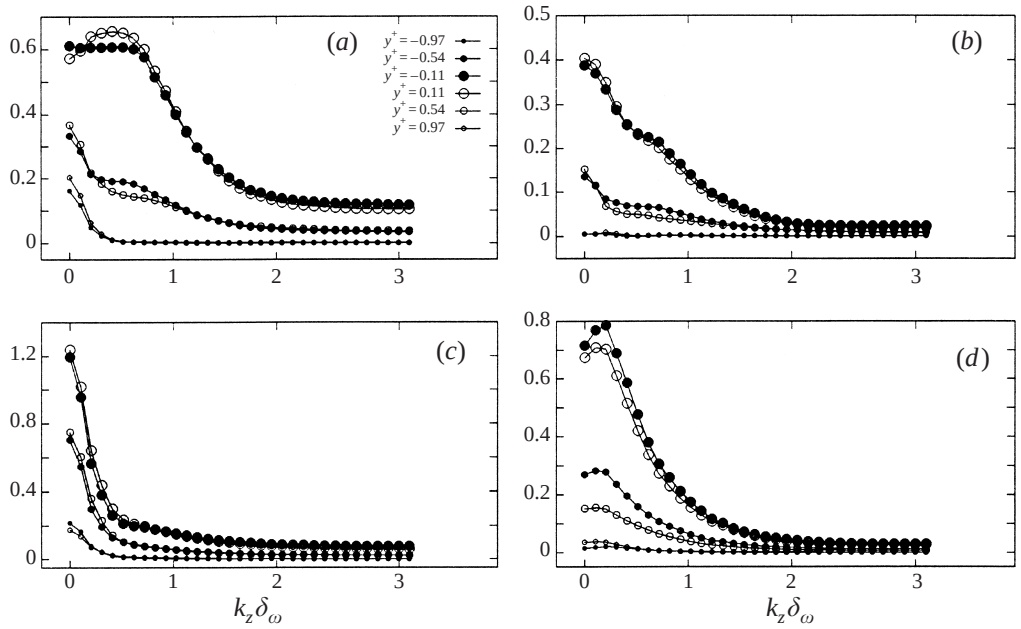

FIGURE 4. Spanwise wavenumber spectra for selected $y^+ = y/\delta_\omega$ locations: (*a*) B_{11}, (*b*) B_{12}, (*c*) B_{22}, (*d*) B_{33}.

dimensional spanwise organization of the flow, which one would expect to have a large correlation length in the spanwise direction.

Near the mixing layer axis R_{11} decays rapidly when the spanwise distance increases, with a negative dip for spatial separations of δ_z/δ_ω in the range [0.5;1.5]. It is interesting to note that the R_{33} correlation behaves very similarly to that of R_{11} although the negative dip is less pronounced and appears for greater spanwise separations. For these correlations, this is indicative of the existence in this region of a preferred organization in the spanwise direction. For all y locations, R_{22} appears to hold its correlation better over the z-direction and never goes negative, indicative of the primarily two-dimensional spanwise structure. R_{12} behaves as a cross between R_{11} and R_{22}, by decaying at rate similar to that of the u-component then levelling out similarly to the v-component. For all of the plots, the energy level at the centre of the mixing layer overwhelms the level at the outer regions of the mixing layer (compare $y^+ \simeq \pm 0.1$ to $y^+ \simeq \pm 1$).

3.2.2. *Spectral tensor*

The results arising from the correlations analysis are indicative of the complex organization of this flow. In order to add to the quantitative description of the flow organization, two quantities are examined in this section: first, the spanwise wavenumber spectra $B_{ij}(y, y' = y, k_z)$ which are obtained by integrating Ψ_{ij} over frequency and, secondly, the Ψ_{ij} spectra themselves.

Plotted in figures 4(*a*) to 4(*d*) is the modulus of selected spectra B_{ij} for $ij = 11$, 12, 22 and 33, respectively.

In the outer region (i.e. $|y^+| > 0.5$), each spectrum, B_{11}, B_{22} and B_{33}, has the same characteristic behaviour where the maximum energy is found at the smallest measured spanwise wavenumber. For this wavenumber, the maxima of B_{11} and B_{22} are of the

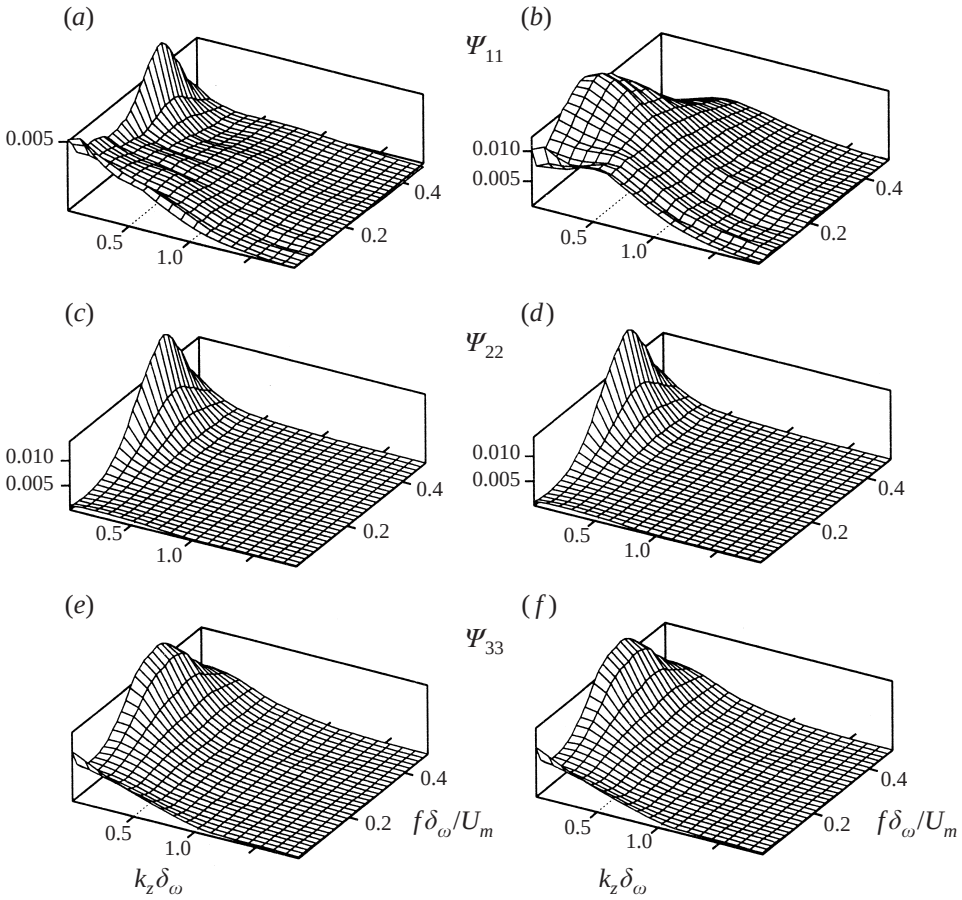

FIGURE 5. $\Psi_{ii}(y, y'; f, k_z)$: (a, c, e) outer region of the mixing layer $(y = y' = 0.5\delta_\omega)$; (b, d, f) inner region $(y = y' = 0.1\delta_\omega)$.

same magnitude and about ten times greater than that of B_{33}. Similarly to the analysis of the correlations, this behaviour is indicative of the predominant flow organization in the spanwise roller region. This is expected because the organization here is highly two-dimensional (mostly involving the u- and v-components). B_{12} in this region is relatively flat implying that the level of correlation is fairly continuous along the spanwise structure.

In the inner part of the mixing layer (i.e. $|y^+| < 0.5$) the spanwise spectra exhibit a different behaviour depending on the velocity component under consideration. Spanwise spectra B_{22} and B_{12} still have their maxima located at the smallest available wavenumber. The energy of B_{22} at this wavenumber is then twice that of the other spectra and drops off rapidly by wavenumbers $k_z\delta_\omega \simeq 0.5$, indicating that the predominance of energy associated with the v-component originates from the spanwise organization. Spectra B_{11} and B_{33} have their maxima at wavenumbers $k_z\delta_\omega \simeq 0.5$ and 0.3, respectively. This representative maxima of energy for these components in the mixing layer is not associated with the spanwise organization, but with a streamwise flow organization, providing the typical streamwise scale is known to be of the order of $2\delta_\omega$ (e.g. Bernal & Roshko 1986). B_{12} has a much slower decay as brought in from the u-component.

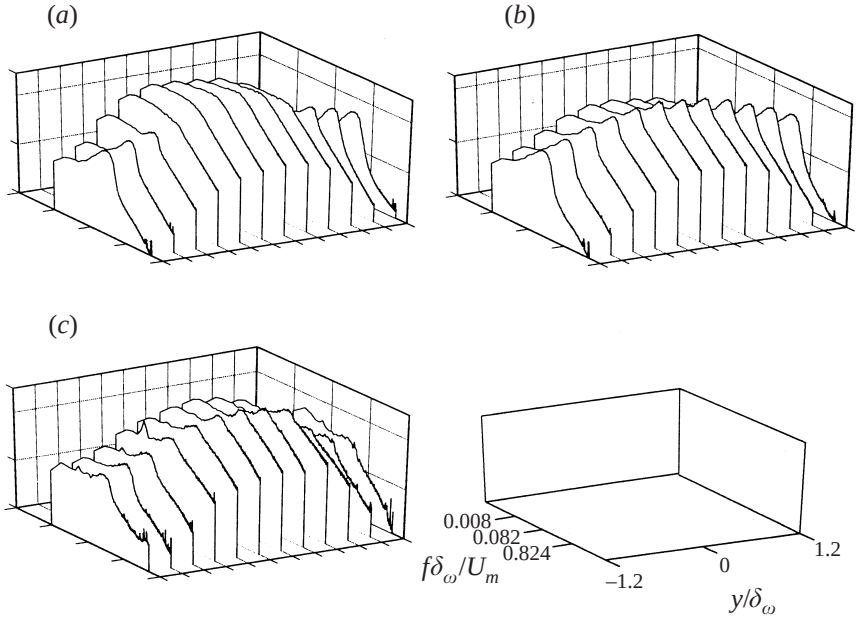

FIGURE 6. Evolution of autospectra $E_i(y;f)$: (*a*) E_1, (*b*) E_2, (*c*) E_3.

In figure 5 the spectra $\Psi_{ij}(y, y' = y; f, k_z)$ are plotted for two y-locations: near the centre of the mixing layer and just past the edge of the mixing layer.

Near the centre of the mixing layer ($y^+ = -0.11$) the u, v and w autospectra have their maxima of energy at different wavenumber/frequency locations as seen in figures 5(*b*), 5(*d*) and 5(*f*). For Ψ_{11}, a dominant wavenumber in z ($k_z\delta_\omega = 0.5$) and a dominant frequency ($f\delta_\omega/U_m = 0.15$) are obtained. This feature corresponds to the two main flow organizations present in the plane mixing layer: large-scale quasi-two-dimensional structures and streamwise aligned vortices. The maximum of energy is located in a region near the intersection of these two wavenumbers. This maximum is relatively broad band when compared with Ψ_{22}. For this spectrum, the footprint of the spanwise organization is strongly dominant; and the maximum of energy is located at the lowest spanwise wavenumber measured. A sharp peak on the frequency axis is found to be at $f\delta_\omega/U_m = 0.3$ which is approximately the typical Strouhal number that is found for the two-dimensional large-scale structures passing through the mixing layer (Browand & Ho 1983). The amplitude of the maximum of Ψ_{22} spectrum is about ten times that of Ψ_{11}; however, the integrated values remain of the same order of magnitude as can be seen from the analysis of B_{ij}.

In the outer region of the mixing layer, the autospectra for u, v and w present the same characteristics as observed for the v-component near the centre of the mixing layer (figures 5*a*, 5*c* and 5*e*). Only the footprint of the large-scale structures, i.e. a peak in the frequency axis of $f\delta_\omega/U_m \simeq 0.3$, is observed. Note that the magnitude of Ψ_{22} is greater than that of Ψ_{11} which is, in turn, greater than that of Ψ_{33}. One would expect the energy in the ww spectrum to be comparatively small in the outer region because as stated before the flow organization in this region is mainly two-dimensional.

Figure 6 summarizes the evolution of the autospectra as a function of the y-direction. The values plotted in this figure, $E_i(y;f)$, can be obtained by integrating the Ψ_{ij} quantities over the spanwise direction. All of the trends of the y-direction

mentioned in the previous discussion of Ψ_{ij} can easily be observed in this figure. It has been found, in Delville *et al*. (1993), that evidence of the streamwise aligned vortical structures can only be observed in the region of $|y| \leqslant \delta_\omega/2$, yet evidence of the spanwise organization can be observed in the spectra at all y-locations. However, it should be noted that, for u near the centre of the mixing layer and w in the outer region, the frequency pointed out corresponds to about half the typical Strouhal number. Relating this to the observations of Metcalfe *et al*. (1987) where they argue that the three-dimensionality originates from the centre of the spanwise vortex tubes, one can extrapolate that the energy associated with these wavenumbers will play a crucial part in achieving three-dimensionality in the dynamical systems model.

4. POD analysis

The proper orthogonal decomposition (POD), which is based on the Karhunen–Loeve expansion (Loeve 1955), was proposed by Lumley (1967) as a *non-prejudice* technique for studying the structure of turbulent flows. The derivation of the governing equations can be found in many places, for example, Berkooz *et al*. (1993). A brief summary is given below.

4.1. *Definition*

Lumley proposed that the candidate structure, $\boldsymbol{\phi}$, be selected so that it is the structure with the largest mean-square projection on the velocity field. This projection process maximizes the energy content of the candidate structure:

$$\max_{\phi} \frac{\langle |(\boldsymbol{u}, \boldsymbol{\phi})|^2 \rangle}{(\boldsymbol{\phi}, \boldsymbol{\phi})} \tag{4.1}$$

where $\boldsymbol{u}$ is the instantaneous velocity field. The inner product is defined as $(f, g) = \int_\Omega f(x) g^*(x) \mathrm{d}x$, where Ω is a space–time domain ($\Omega = \mathscr{D} \times \mathscr{T}$). Equation (4.1) is normalized by $(\boldsymbol{\phi}, \boldsymbol{\phi})$ which removes its dependence on amplitude since we are interested in the degree of projection and not the amplitude.

Maximizing this mean-square energy projection can be done by the calculus of variations (Lumley 1981) or by defining a Hermitian operator (Berkooz 1991). This leads to the following integral eigenvalue problem:

$$\int_\Omega R_{ij}(\boldsymbol{x}, \boldsymbol{x}', t, t') \psi_j(\boldsymbol{x}', t') \, \mathrm{d}\boldsymbol{x}' \, \mathrm{d}t' = \lambda \psi_i(\boldsymbol{x}, t), \tag{4.2}$$

where the kernel is the velocity cross-correlation tensor, $R_{ij}(\boldsymbol{x}, \boldsymbol{x}', t, t') = \langle u_i(\boldsymbol{x}, t) u_j(\boldsymbol{x}', t') \rangle$ and the eigenvalue, λ, is representative of the integrated turbulent kinetic energy. Since R_{ij} is a symmetric positive definite function, the solutions to (4.2) can be discussed using the Hilbert–Schmidt theory (Lumley 1967).

One of the more interesting artifacts of the Hilbert–Schmidt theory is that an infinite number of orthonormal solutions can be used to express the original instantaneous velocity field $u_i(\boldsymbol{x}, t)$ as

$$u_i(\boldsymbol{x}, t) = \sum_{n=1}^{\infty} u_i^{(n)}(\boldsymbol{x}, t), \qquad \text{where} \quad u_i^{(n)}(\boldsymbol{x}, t) = a^{(n)} \psi_i^{(n)}(\boldsymbol{x}, t), \tag{4.3}$$

and

$$a^{(n)} = \int_\Omega u_i(\boldsymbol{x}, t) \psi_i^{(n)*}(\boldsymbol{x}, t) \, \mathrm{d}\boldsymbol{x} \, \mathrm{d}t. \tag{4.4}$$

If a direction in the flow field is assumed to be statistically stationary or homogeneous, the POD reduces to the harmonic decomposition theorem (see Lumley 1967 or George 1988). This implies that the eigenfunctions are harmonic functions and can be handled through Fourier analysis first. Introducing this Fourier transform leads to a phase indetermination problem, where the description of the POD modes becomes local in Fourier space and non-local in physical space. Retrieving the POD modes in physical space is then limited by two points: first, the solution for the integral in (4.4) implies that the velocity field is known at all locations simultaneously (which cannot be done easily in an experimental approach) and, second, the 'phase indetermination' has to be solved. Complementary techniques such as the shot-noise decomposition (Lumley 1981) or dynamical models (Aubry *et al*. 1988) can be utilized for determining the a, hence the reconstruction of the POD modes contribution by using (4.3).

4.2. *POD application to the mixing layer*

The POD in the mixing layer was solved for two different cases. In the first application $\Psi_{ij}(y, y'; f, k_3)$, where $i = 1, 2$ and $j = 1, 2$, is used as the kernel for the integral eigenvalue problem. Because of spanwise homogeneity the third component (w) is more or less uncoupled from u and v. For example correlations such as $R_{13}(y, y'; 0, 0)$ are zero. Given this it is expected that taking into account only u and v leads to interesting results, in terms of flow organization. This decomposition will be called 2.5D-POD and is only briefly discussed in this communication. Details can be found in Delville & Ukeiley (1993). It should be noted that in this first decomposition there is no implementation of Taylor's hypothesis. In the second application, which is discussed in § 5.2, Taylor's hypothesis and the continuity equation are used to build the full spectral correlation tensor $\boldsymbol{\Psi}_{ij}(y, y'; k_1, k_3)$ for $i = 1, 2, 3$ and $j = 1, 2, 3$, which is then decomposed. This last decomposition will be called 3D-POD. Note that in the following, k_1 (or k_x) and k_3 (or k_z) correspond to the streamwise and spanwise wavenumbers, respectively.

The use of Taylor's hypothesis to map the frequency to streamwise wavenumbers involves implicitly two assumptions: first the existence of a convection velocity and secondly homogeneity in the streamwise direction. The way the convection velocity is used will be detailed and discussed in § 5.1. The suggested local homogeneity in the streamwise direction is an approximation and can be subject to criticism. It can be shown that with this assumption no expansion can be found for the downstream evolution of the flow. However, if one remains in a local framework, a useful approximation can be obtained for at least two aspects of the flow: the typical scales and typical organization. Checking the influence of this assumption on the results obtained would require measurements involving streamwise spatial separations. Although it is not possible to examine this assumption with the database reported in this study, work with numerical simulations have been conducted by Cordier, Delville & Tenaud (1997). In that study the space–time correlations obtained directly from the simulation were found to be in agreement with the experimental ones obtained by the process involved in the present paper: the only difference between the two sets of correlations was that, for downstream separations, the transversal extent (y-direction) of constant correlation contours is found to be symmetric when homogeneity is assumed while this varies with downstream distance when homogeneity is not.

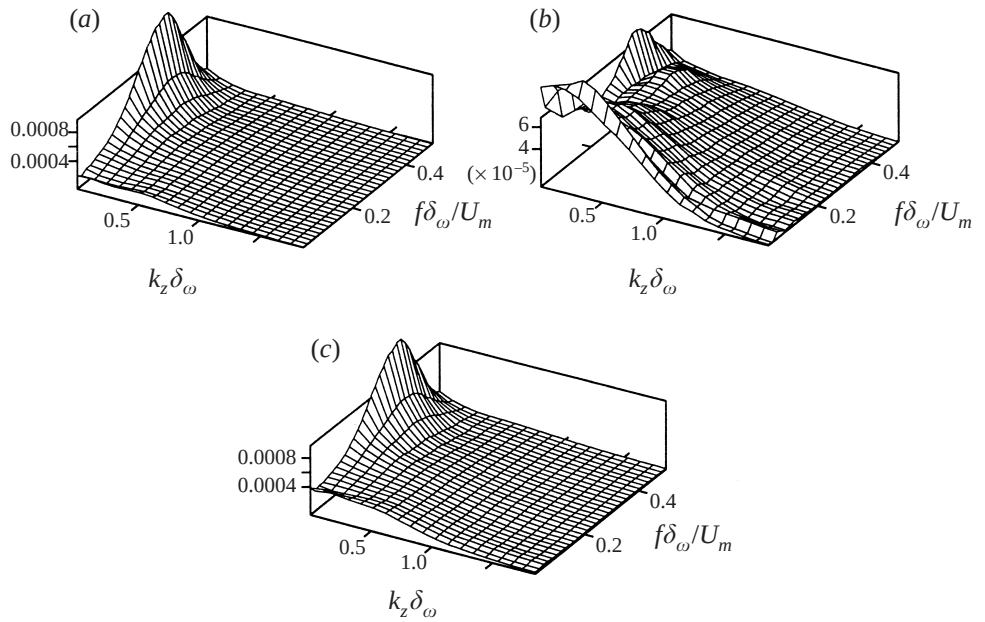

FIGURE 7. Eigenspectra (*a*) $\lambda^{(1)}$, (*b*) $\lambda^{(2)}$, (*c*) $\sum_n \lambda^{(n)}$ for 2.5D-POD.

4.3. *Analysis of 2.5D-POD modes*

In the mixing layer flow studied here, the time 'direction' is statistically stationary and the spanwise direction is assumed to be locally homogeneous. The cross-correlation tensor $R_{ij}(\boldsymbol{x}, \boldsymbol{x}', t, t')$ in (4.2) is then decomposed using a Fourier transform resulting in

$$R_{ij}(\boldsymbol{x}, \boldsymbol{x}', t, t') \Longrightarrow \Psi_{ij}(y, y'; f, k_3), \tag{4.5}$$

where Ψ_{ij} is the cross-spectral tensor dependent on frequency and spanwise wavenumber. Details of the calculation of this quantity were discussed in § 3.1. The integral eigenvalue of (4.2) now becomes

$$\int_{-L_y/2}^{L_y/2} \Psi_{ij}(y, y'; f, k_3)\Phi_j^{(n)}(y'; f, k_3)\,\mathrm{d}y' = \lambda^{(n)}(f, k_3)\Phi_i^{(n)}(y; f, k_3), \tag{4.6}$$

where Φ_1 (or Φ_u) and Φ_2 (or Φ_v) are now frequency and spanwise-wavenumber dependent eigenfunctions, $\lambda^{(n)}(f, k_3)$ represents the eigenspectra, and y denotes the remaining inhomogeneous direction. This equation, in the case of the 2.5D-POD is solved for $i = 1, 2$ and an implicit summation exists over $j = 1, 2$.

The shape of the dominant eigenvalue spectrum $\lambda^{(1)}(f, k_3)$ as shown in figure 7(*a*) is very similar to the union of the two individual Ψ_{ii} measured near the mixing layer axis for $y^+ = -0.11$ (figure 5). The peak at $f\delta_\omega/U_m = 0.3$ as seen in Ψ_{22} and less pronounced the maximum at $k_z\delta_\omega = 0.5$ of Ψ_{11} (both near the centre of the mixing layer axis) are discernible in figure 7(*a*). A juggling between the influence of the v- and u-components can be seen: v dominates in the first few spanwise wavenumbers and u in the others. The 'dominant mode' can then be split into two spanwise wavenumber domains: the lowest wavenumbers can be related to the large quasi-two-dimensional structures for which v is found dominant, and the higher wavenumbers where the three-dimensional aspect of the organization of the flow is carried essentially by the

u component. This suggests that the 'coherent structure' is a combination of the two main organizations observed in this flow.

When the first POD mode is integrated over f, 80% of its energy is contained in the smallest k_z. The overall contribution of the first mode to the energy can be obtained when integrating over all the wavenumbers and frequencies. The first mode of the POD plotted in figure 7(a) contains about 53% of the energy (80% for the summation over the first three modes). The values obtained here are greater than those from the vectorial POD_{uv} where no spanwise separation is examined. In that case, only 41% of the energy is contained in the first mode and 71% in the first three modes (Delville 1994). This result confirms that taking into account more information from the flow (here adding spanwise dependency) leads to a first POD mode that better represents the flow. The good representation of the first mode can also be found by comparing the eigenvalue for the first mode in figure 7(a) to the summation of all the modes of the POD plotted in figure 7(c). This makes it clear that the first mode contains most of the information in the energy-containing (f, k_z) pairs.

It is interesting to note that in figure 7(b) the streamwise organization dominant for the second POD mode is contrary to what occurs for the first mode. For $\lambda^{(2)}$ the peak in f is at the same frequency as for $\lambda^{(1)}$; however, the peak in k_z is located at $k_z\delta_\omega = 0.25$. It has been shown (see Delville *et al*. 1993) that this typical wavenumber corresponds to the characteristic spanwise wavenumber that is observed near the edges of the mixing layer. This indicates that the second POD mode captures information preferentially from these regions. Also note that the first mode of the POD carries information from this region as well.

In order to be able to give the 'coherent structure' a physical representation (i.e. in space/time and not in the wavenumber/frequency domain), it is necessary to use complementary tools (e.g. shot noise as will be discussed in § 6 or dynamical systems model which will be discussed later in Part 2). This is due to the fact that by using the cross-spectral tensor as the kernel of the eigenvalue problem, the phase in the directions where the Fourier transforms are applied is lost. However, the information about the phase in the inhomogeneous direction y can be accessed because it is contained in the eigenfunctions. Nevertheless, we can hope to find topological information about the organization of the structure in the inhomogeneous direction as well as the distribution of scales from examining the eigenfunctions. This has been done and reported in Delville & Ukeiley (1993) for the 2.5D-POD. In § 5.2 the shape of the eigenfunctions will be discussed for the application of the 3D-POD.

5. Application of continuity and 3D-POD

In this section the application of the continuity equation to the cross-spectral tensor is described, along with the formulation and results of the 3D-POD.

5.1. *Estimation of the entire spectral tensor*

In order to fill in the non-measured parts of the correlation tensor, the continuity equation was used in conjunction with Taylor's hypothesis. In the experiments Ψ_{11}, Ψ_{12}, Ψ_{22}, Ψ_{13} and Ψ_{33} were measured as a function of y, y', f and k_3. First Taylor's hypothesis was used to map these quantities to $\boldsymbol{\Psi}_{11}$, $\boldsymbol{\Psi}_{12}$, $\boldsymbol{\Psi}_{22}$, $\boldsymbol{\Psi}_{13}$ and $\boldsymbol{\Psi}_{33}$ in terms of y, y', k_1 and k_3. The only way to calculate $\boldsymbol{\Psi}_{23}$ is to make use of the continuity equation. The remaining terms (i.e. $\boldsymbol{\Psi}_{21}$, $\boldsymbol{\Psi}_{31}$ and $\boldsymbol{\Psi}_{32}$) were calculated using the following symmetry:

$$\boldsymbol{\Psi}_{ij}(y, y'; k_1, k_3) = \boldsymbol{\Psi}^*_{ji}(y', y; k_1, k_3). \tag{5.1}$$

Taylor's hypothesis is invoked to map the data from frequency to streamwise wavenumber: $k_1 = -f/U_c$, which assumes that the turbulence is frozen and being convected with the mean streamwise convection velocity. This leads to the following relations:

$$\boldsymbol{\Psi}_{ij}(y, y'; k_1, k_3) = U_c \boldsymbol{\Psi}_{ij}(y, y'; f, k_3). \tag{5.2}$$

Defining a convection velocity is a non-trivial task and remains controversial (e.g. Zaman & Hussain 1981, or Leboeuf & Metha 1995). The average convective velocity U_m could be used, but this value must be too large considering the drag shown in the flow patterns. Whatever the value chosen for U_c, the following question is also present: does this convection velocity need to be the same for all the flow scales?

The following paragraphs describe an approach to address the above question based on the use of the continuity equation.

The continuity equation for an incompressible turbulent field can be expressed in terms of the fluctuating velocity as follows:

$$\frac{\partial u_i'}{\partial x_i} = 0. \tag{5.3}$$

This equation can be written in terms of the correlation tensor R_{ij} by

$$\frac{\partial R_{ij}}{\partial x_i} = 0. \tag{5.4}$$

The spectral tensor can be represented as the Fourier transform of the correlation tensor as shown in (3.4) so that the continuity equation becomes

$$2\pi \mathrm{i} k_1 \boldsymbol{\Psi}_{1j} + \frac{\partial \boldsymbol{\Psi}_{2j}}{\partial x_2} + 2\pi \mathrm{i} k_3 \boldsymbol{\Psi}_{3j} = 0. \tag{5.5}$$

Equation (5.5) allows one to express $\boldsymbol{\Psi}_{3j}$ as

$$\boldsymbol{\Psi}_{3j} = \frac{1}{2\pi k_3} \left(-2\pi k_1 \boldsymbol{\Psi}_{1j} + \mathrm{i} \frac{\partial \boldsymbol{\Psi}_{2j}}{\partial x_2} \right). \tag{5.6}$$

In terms of the measured quantities Ψ_{ij}, this equation can be written for $j = 2$:

$$\Psi_{32} = \frac{f}{U_c k_3} \Psi_{12} + \frac{\mathrm{i}}{2\pi k_3} \frac{\partial \Psi_{22}}{\partial x_2}. \tag{5.7}$$

Considering the wavenumber $k_3 = 0$ (i.e. considering the large-scale two-dimensional spanwise aligned motion), the convection velocity arising from (5.7) can be estimated for each (y, y') pair and frequency by using

$$u_c(y, y'; f) \frac{\partial \Psi_{22}}{\partial x_2}(y, y'; f, k_3 = 0) = 2\pi \mathrm{i} f \Psi_{12}(y, y'; f, k_3 = 0). \tag{5.8}$$

If one assumes that the convection velocity U_c is constant across the mixing layer (see Zaman & Hussain 1981), an average convection velocity $U_c(f)$ can be obtained by solving (5.8) using a least-squares approach:

$$U_c(f) = \frac{\displaystyle\int_{-L_y/2}^{L_y/2} \int_{-L_y/2}^{L_y/2} \frac{\partial \Psi_{22}}{\partial x_2}(y, y'; f, k_3 = 0) \times 2\pi \mathrm{i} f \Psi_{12}(y, y'; f, k_3 = 0) \, \mathrm{d}y \, \mathrm{d}y'}{\displaystyle\int_{-L_y/2}^{L_y/2} \int_{-L_y/2}^{L_y/2} \left(\frac{\partial \Psi_{22}}{\partial x_2}(y, y'; f, k_3 = 0) \right)^2 \mathrm{d}y \, \mathrm{d}y'}. \tag{5.9}$$

This quantity, plotted on figure 8 as the ratio U_c/U_m, is close to 0.8 for reduced

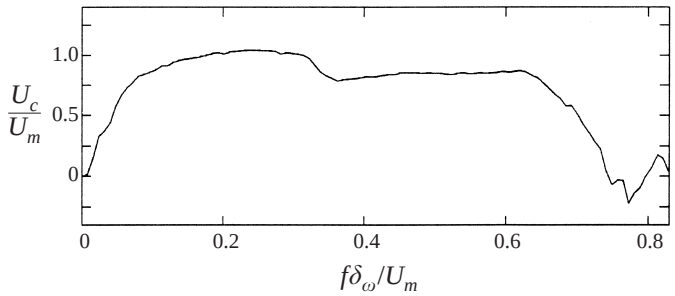

FIGURE 8. Frequency evolution of spatially averaged convection velocity.

frequencies $f\delta_\omega/U_m$ in the range [0.1; 0.7]. This shows that although the convective velocity might not be a constant for all scales, for the scales of interest in this paper and Part 2 it is approximately constant. Hence, the global convection velocity U_c has been chosen to be independent of the frequency (or streamwise wavenumbers) and assumed to be $U_c = 0.8U_m$.

The method used here to estimate the full spectral correlation tensor does not ensure that the continuity relationship is satisfied for the entire system. In fact, the chosen procedure guarantees that the continuity equation will be violated. However, by using this method only for estimating Ψ_{32}, a relatively small term, one can hope the violation is small. Once the POD is solved, the eigenfunctions will be checked to verify the continuity relationship (see § 5.2.1).

5.2. *3-D POD*

Now that all of the components of the correlation tensor have been acquired, the application of the POD can be expanded. For the second application of the POD, denoted 3D-POD, $\Psi_{ij}(y, y', f, k_3)$ was mapped to $\boldsymbol{\Psi}_{ij}(y, y', k_1, k_3)$ through the use of Taylor's hypothesis, as discussed in § 5.1. In this case $i = 1, 2, 3$ and $j = 1, 2, 3$, and the components $\boldsymbol{\Psi}_{23}$ and $\boldsymbol{\Psi}_{32}$ were solved from an application of the continuity equation. The resulting Fredholm equation is then

$$\int_{-L_y/2}^{L_y/2} \boldsymbol{\Psi}_{ij}(y, y'; k_1, k_3)\boldsymbol{\Phi}_j^{(n)}(y'; k_1, k_3)\,\mathrm{d}y' = \boldsymbol{\lambda}^{(n)}(k_1, k_3)\boldsymbol{\Phi}_i^{(n)}(y; k_1, k_3). \tag{5.10}$$

Now the eigenvalues and eigenfunctions are streamwise and spanwise wavenumber dependent.

5.2.1. *Continuity of POD modes*

In this section the use of only a single equation from the continuity relationship will be justified by verifying that the POD eigenfunctions satisfy the continuity relationship. Since the eigenfunctions themselves are representative of an incompressible flow, they should be divergence free. The continuity equation for the eigenfunctions can be written as $\mathrm{d}\boldsymbol{\Phi}_i^{(n)}/\mathrm{d}x_i = 0$. Since the eigenfunctions that are solved for in (5.10) are in Fourier space, this equation can be rewritten as

$$D^{(n)}(y; k_1, k_3) = 2\mathrm{i}\pi k_1 \boldsymbol{\Phi}_1^{(n)} + \frac{\mathrm{d}\boldsymbol{\Phi}_2^{(n)}}{\mathrm{d}x_2} + 2\mathrm{i}\pi k_3 \boldsymbol{\Phi}_3^{(n)} = 0. \tag{5.11}$$

Figure 9 is a typical plot, for the first POD mode, of the maximum for all y of $|D(y; k_1, k_3)|$, the solution of (5.11), and is indicative of the divergence of the eigenfunctions. The values in this plot are normalized by $\Delta U/\delta_\omega$ and are plotted as

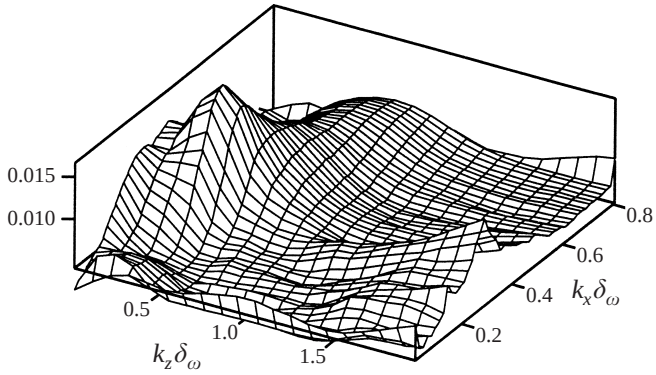

FIGURE 9. Typical divergence of eigenfunctions. Plotted is $\max[|D(y;k_1,k_3)|]_y/(\Delta U/\delta_\omega)$.

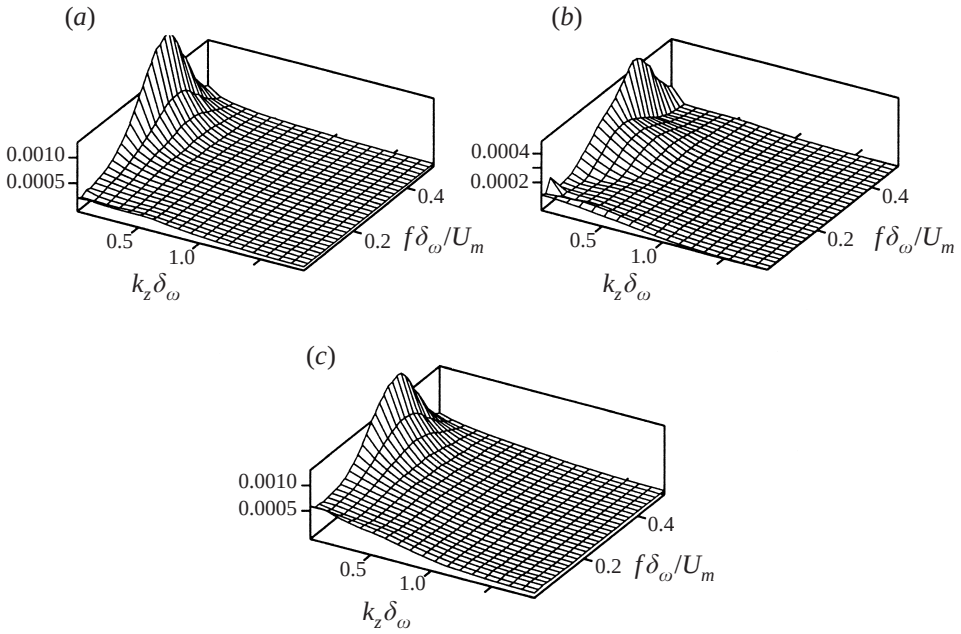

FIGURE 10. Eigenspectra (*a*), $\lambda^{(1)}$, (*b*) $\lambda^{(2)}$, (*c*) $\sum_n \lambda^{(n)}$ for 3D-POD.

a function of k_x and k_z. The maximum value of the divergence has been found to be approximately 2% with the average $\simeq 0.6\%$. This result is quite satisfactory for the present application.

In hindsight this result is not that surprising if one considers that the only term calculated from the application of continuity was Ψ_{32}. In general this term's contribution to the spectral tensor is small, thus it should only introduce a small error.

5.2.2. *Eigenvalues and eigenfunctions*

As with application of the 2.5D-POD, the convergence of the modes was found to be rapid. This is evident when comparing in figures 10(*a*) and 10(*c*) the first POD mode to the summation of all the modes or the difference of scales between mode 1 and mode 2 in figures 10(*a*) and 10(*b*). The first mode contained 49% of the turbulent kinetic energy with 99% being represented by the summation of the first seven modes.

The shape of $\sum_n \boldsymbol{\lambda}^{(n)}(k_x, k_z)$, as shown in figure 10(*c*), is very similar to that of the 2.5D-POD case in figure 7(*c*). The most observable difference is that the values in the low spanwise/streamwise wavenumber corner (the region representative of the centre of the mixing layer bounded by $k_x\delta_\omega \simeq 0.2$ and $k_z\delta\omega \simeq 0.5$ of figure 5*b*) appear to be greater for the 3D-POD (i.e. 6×10^{-4} compared to 4×10^{-4}). If one considers that the eigenvalues are the integrated energy over the domain, this shows that the main contribution from the third velocity component should be in this low-wavenumber area. This is consistent with the results obtained by Zheng & Glauser (1991) where it was found that the addition of the third component highlighted information that was characteristic of the secondary structures. The shape of the dominant mode $\boldsymbol{\lambda}^{(1)}(k_x, k_z)$ in figure 10(*a*), as with the 2.5D-POD application, exhibits all of the main characteristics shown by the summation of all the POD modes. The shape of $\boldsymbol{\lambda}^{(2)}$ appears to be significantly different from that for the 2.5D-POD application, where it was found to be more representative of the spanwise organization. For this application, the shape is very similar to that of the first mode, but with a more broad-band peak at the lowest spanwise wavenumber.

The following discussion concentrates on the behaviour of the eigenfunctions for the first mode of the POD only. Specifically, the spanwise wavenumbers pointed out in § 3.2.2 are analysed: $k_{z3} \simeq 0.3\delta_\omega^{-1}$, $k_{z5} \simeq 0.5\delta_\omega^{-1}$ and $k_{z1} \simeq 0.1\delta_\omega^{-1}$. One should recall that k_{z3} is typical of the organization near the edge of the mixing layer while k_{z5} is typical of the organization near the centre of the mixing layer. The smallest spanwise wavenumber in this experiment k_{z1} is also examined in order to get an idea of the large-scale two-dimensional behaviour of the 'structure' (i.e. corresponding to the largest spanwise extent). The modulus of the eigenfunctions, which are complex functions, are plotted on figure 11, weighted by the square root of the corresponding eigenvalue. The shapes of $\boldsymbol{\Phi}_1$ and $\boldsymbol{\Phi}_2$ exhibit similar trends to those observed for the 2.5D-POD reported in Delville & Ukeiley (1993). All the plots of this figure exhibit a symmetry relative to the mixing layer axis ($y = 0$) as could be inferred from the symmetric nature of the energy profile. Large differences can be found in the behaviour of the eigenfunctions $\boldsymbol{\Phi}_1$ for the selected wavenumbers. For this eigenfunction, the three spanwise wavenumbers considered exhibit a quite different behaviour. When looking at k_{z1}, three maxima can be found: one primary maximum on the mixing layer axis and two symmetrical secondary maxima located at $|y^+| \simeq 0.7$. For the higher spanwise wavenumber, only the primary maximum on the mixing layer axis remains. These maxima are located at the centre of the mixing layer at $k_x\delta_\omega \simeq 0.15$ and near the edge of the mixing layer at $k_x\delta_\omega \simeq 0.3$. Whatever the spanwise wavenumber, for $\boldsymbol{\Phi}_2$ there is only one maximum, located in the centre of the mixing layer at $k_x\delta_\omega \simeq 0.3$. It was observed for this eigenfunction that, for each spanwise wavenumber considered, the order of magnitude of the imaginary part remains small when compared to the modulus; this implies that the v-component of the structure remains in phase over the y-direction whatever the spanwise wavelength considered. The shape of $\boldsymbol{\Phi}_3$ for $k_z\delta_\omega \simeq 0.1$ exhibits two maxima located at $k_x\delta_\omega \simeq 0.3$. In the y-direction the maxima are located just on either side of the mixing layer axis. This figure also indicates that, for larger values of the spanwise wavenumber, $\boldsymbol{\Phi}_3$ behaves similarly to $\boldsymbol{\Phi}_2$.

A quite simple physical scheme for the organization of the flow field can be given in order to explain these features. The three local maxima observed for $\boldsymbol{\Phi}_1$ are due to the mixing of the symmetric properties of the real part and the antisymmetric properties of the imaginary part of the eigenfunctions that can be induced from the 'large-scale behaviour' of the flow. The large-scale organization can be related, for this flow following conventional conditional approaches, to an increase of the

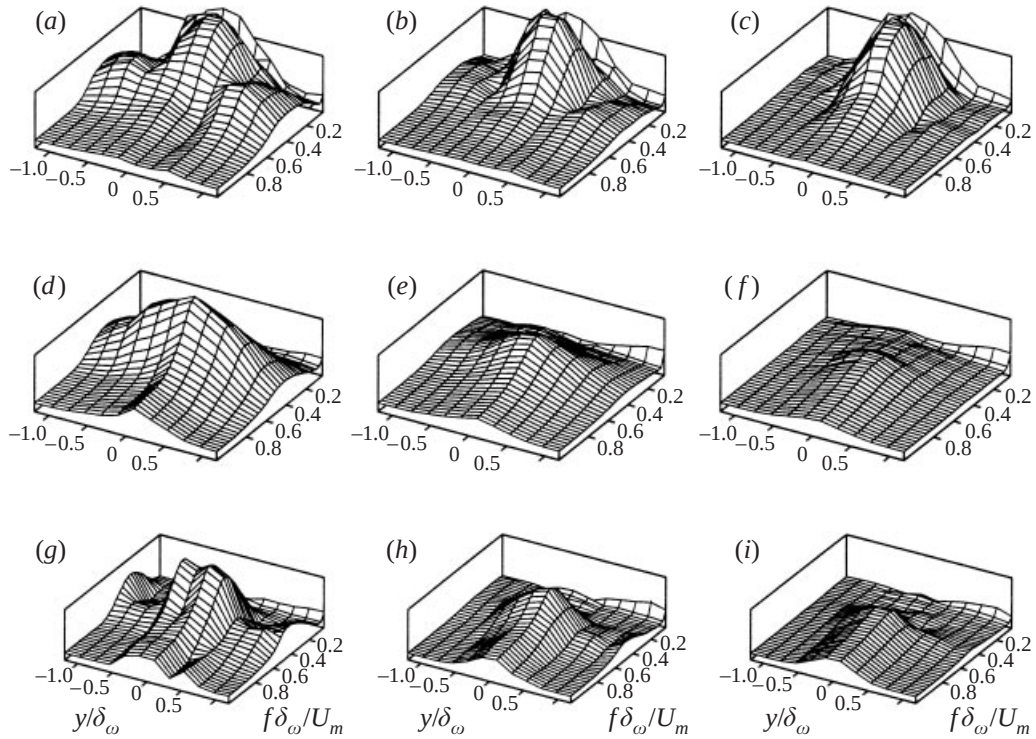

FIGURE 11. Modulus of eigenfunction $\boldsymbol{\Phi}_i^{(1)}$ for 3D-POD: (*a–c*) $\boldsymbol{\Phi}_1$, (*d–f*) $\boldsymbol{\Phi}_2$, (*g–i*) $\boldsymbol{\Phi}_3$.

velocity in the high-velocity side of the mixing layer associated with decreases of velocity in the low-velocity side of the mixing layer. This organization can then be related to the spatial phase opposition between the two external parts of the mixing layer. This behaviour expressed in terms of the eigenfunctions can be translated into anti-symmetrical behaviour (odd function in y). In the complex space, this behaviour is related to a dominating odd imaginary part (in the y-direction); however the modulus as plotted in figure 11 appears as positive maximum. The primary maxima at $k_x\delta_\omega \simeq 0.15$ corresponds to the symmetric real part of the eigenfunctions. This symmetry is related to the maximum of energy located on the axis of the mixing layer as discussed earlier. One can, in this context, relate the behaviour of $\boldsymbol{\Phi}_1$ for the selected spanwise wavenumbers to the following characteristics. For $k_z = k_{z3}$ or $k_z = k_{z1}$ there are two distinct frequency domains. In the area of $f\delta_\omega/U_m = 0.15$ the flow organization associated with the energy on the axis is observed; while in the range of $k_x\delta_\omega = 0.3$ the characteristics associated with the passage of the quasi-two-dimensional organization is observed. However, for higher spanwise wavenumbers (i.e. $k_z = k_{z3}$) only the organization associated with the energy on the axis is observed. In the same vein the two maxima noticed for $\boldsymbol{\Phi}_3$ are actually of opposite sign if their real and imaginary parts are examined. Using geometric arguments, one can think of streamwise vortex tubes as represented by opposing vectors in the z-direction.

5.2.3. *Energy profiles*

The contributions from the first two modes to the energy profiles are shown in figure 12. The first mode represents the profiles well for all the cases. It is particularly efficient for $v'v'$ and for $u'v'$ as well. Considering the $u'v'$ Reynolds stress, it is

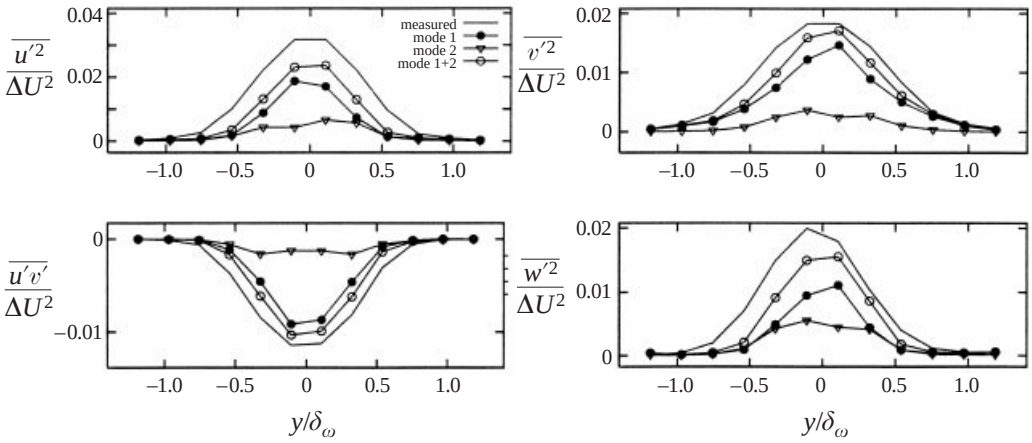

FIGURE 12. Contribution of the POD modes to the Reynolds stresses for 3D-POD.

interesting to point out that in several previous comparable studies involving k_x and k_z dependence, (e.g. Moin & Moser 1989 and Glauser & George 1987) the Reynolds stress was found to be very representative, even leading to an over-estimation of the first or second mode. In this study, however, this behaviour was not observed. It is evident from these figures that the convergence is more rapid near the centre of the mixing layer. One would expect this since the decomposition is based on energy and areas of high energy will converge the most rapid.

5.2.4. *Reconstruction of spectra*

Figure 13 presents the contribution of the first 3D-POD mode to the autospectra at $y = 0.1\,\delta_\omega$ and $y = 0.5\,\delta_\omega$ for u, v and w, respectively. The u and v autospectra show the same global features as the original autospectra plotted in figure 5. This demonstrates the effectiveness of the POD for representing the important features (on an energy-weighted basis) of the flow. For the autospectra of w, the overall characteristics at wavenumbers greater than $k_x\delta_\omega \simeq 0.3$ seem to be well represented by the first POD mode. However, in the low spanwise/streamwise wavenumber corner the energy is significantly under represented. These global features are consistent with the results from the examination of the eigenspectra (figure 10) which showed that the first mode represents the energy contained in the flow accurately.

6. Reconstruction in physical space

In the previous Sections, it has been shown that the spectral distribution of dominant scales characteristic of the flow organization can be retrieved from the first POD mode. However, the phase indetermination due to the use of Fourier transforms in the homogeneous and stationary directions implies that a physical space description of this mode cannot be obtained directly. An explicit physical description of the dominant mode can only be obtained in the y-direction, for which the POD was applied. For directions x and z this description is known only in the spectral domain. Therefore this description is globally non-local in physical space. The aim of this Section is to provide a physical description of the dominant POD mode, i.e. $\boldsymbol{\Phi}_i^{(1)}$, in terms of space variables $(x,\ y,\ z)$ following Lumley (1981).

Two approaches can be used in order to gain a description in physical space. A

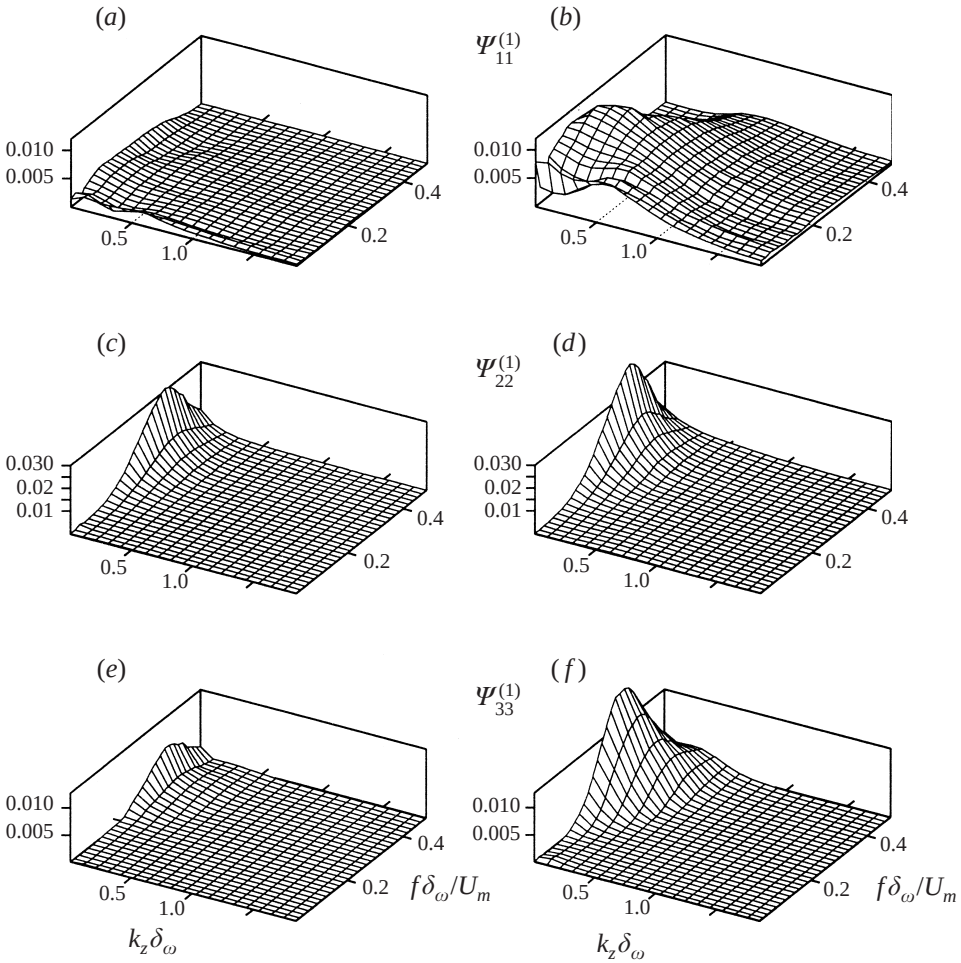

FIGURE 13. Contribution of the first mode of 3D-POD to $\boldsymbol{\Psi}_{ii}$: (a, c, e) $y = 0.5\delta_\omega$; (b, d, f) $y = 0.1\delta_\omega$.

'static' description of the dominant mode can be obtained by using a complementary theory: *the shot-noise theory*. This specific approach will be discussed and developed in the following Sections. An alternative way is to build, from the dominant eigenfunctions, a low-order model by use of a Galerkin projection of governing equations onto the POD modes, leading to a low-order dynamical system (through a set of ODEs). In this case, these equations themselves drive the missing spectral phase information. However, additional hypotheses concerning spectral symmetries, influence of neglected higher modes, and relationship with the 'mean' flow will be required. By this Galerkin projection procedure, a dynamical description of the flow is also obtained, and this approach will be addressed in Part 2.

6.1. *Phase indetermination*

To describe the dominant mode in physical space, it is necessary to obtain a description of the expansion coefficients appearing in (4.3). In the case of the 3D-POD, these equations can be written by considering only the first mode (1):

$$u_i^{(1)}(x, y, z) = \int a^{(1)}(\boldsymbol{K})\boldsymbol{\Phi}_i^{(1)}(y; \boldsymbol{K}) \exp(2i\pi(\boldsymbol{K} \cdot \boldsymbol{X}))\, d\boldsymbol{K}, \tag{6.1}$$

where $\boldsymbol{K} = (k_x, k_z)$ and $\boldsymbol{X} = (x, z)$. Coefficients $a^{(1)}(\boldsymbol{K})$ are obtained from

$$a^{(1)}(\boldsymbol{K}) = \int \widetilde{u_i}(y;\boldsymbol{K})\boldsymbol{\Phi}_i{}^{*(1)}(y;\boldsymbol{K})\,\mathrm{d}y, \tag{6.2}$$

where $\widetilde{u_i}(y;\boldsymbol{K})$ is the Fourier transform of the flow field in the homogeneous directions x and z.

Considering the relation $\langle a^{(1)}(\boldsymbol{K})a^{(1)*}(\boldsymbol{K})\rangle = \boldsymbol{\lambda}^{(1)}(\boldsymbol{K})$ one can estimate the modulus of $a^{(1)}$ as the square root of the eigenvalue. The same consideration was used in the normalization describing the eigenvectors in the previous Section (e.g. see figure 11).

However, it can easily be shown that if the eigenfunction $\boldsymbol{\Phi}_i(y;\boldsymbol{K})$ is a solution of the eigenvalue problem, any function such as $\boldsymbol{\Phi}_i(y;\boldsymbol{K})\mathrm{e}^{\mathrm{i}\Theta(\boldsymbol{K})}$ is also solution of this problem (note that the phase function Θ introduced is independent of the velocity component i). Therefore a phase indetermination exists and needs to be solved.

6.2. *'Shot-noise' decomposition*

Several methods used to solve the phase indetermination involve a generalization of the 'shot-noise' theory initiated by Rice (1954). This theory provides a formalism to estimate the coefficient $a^{(1)}$. In this decomposition, the random field is considered as being built up from non-overlapping characteristic eddies randomly distributed in the homogeneous directions. The shot-noise decomposition can be written

$$u_i{}^{(1)}(x, y, z) = \int \mathscr{U}_i(\boldsymbol{X} - \boldsymbol{X}')g(\boldsymbol{X}')\,\mathrm{d}\boldsymbol{X}'. \tag{6.3}$$

In this equation, the deterministic functions $\mathscr{U}_i$ sought are representative of the large eddies in physical space and g is a random function representative of the distribution (amplitude and occurrence) of these eddies in the homogeneous directions. By comparing the two descriptions of the random field (equations (6.3) and (6.1)), considering the Fourier transform of these equations and using the convolution theorem, it can be easily shown that

$$\widetilde{\mathscr{U}_i}(y;\boldsymbol{K})\widetilde{g}(\boldsymbol{K}) = a^{(1)}(\boldsymbol{K})\,\boldsymbol{\Phi}_i^{(1)}(y;\boldsymbol{K}). \tag{6.4}$$

By considering the product with its conjugate of the previous equation, and introducing an ensemble average and $E_g(\boldsymbol{K})$, the spectrum of the distribution function of g (equation (6.6)), the spectral description of $\mathscr{U}_i$ can be obtained:

$$\widetilde{\mathscr{U}_i}(y;\boldsymbol{K}) = \left[\frac{\boldsymbol{\lambda}^{(1)}(\boldsymbol{K})}{|E_g(\boldsymbol{K})|}\right]^{1/2} |\boldsymbol{\Phi}_i^{(1)}(y;\boldsymbol{K})|\ \ \mathrm{e}^{\mathrm{i}\Theta(\boldsymbol{K})}. \tag{6.5}$$

The dominant structure reconstruction could be obtained in physical space by the inverse Fourier transform of (6.5), providing E_g is known.

Lumley (1981) proposed developing the distribution function g as an infinite sum of Dirac functions with amplitude A_α, randomly distributed in the homogeneous directions:

$$g(\boldsymbol{X}) = \sum_\alpha A_\alpha \delta(\boldsymbol{X} - \boldsymbol{X}_\alpha). \tag{6.6}$$

With the hypothesis that consecutive events are non-overlapped and the amplitude and distribution of g are not correlated, it can be shown that the spectrum E_g is real, positive and independent of the wavenumbers $\boldsymbol{K}$:

$$E_g(\boldsymbol{K}) = \langle A_i^2\rangle/\mu,$$

where μ is the average time delay between two successive events. One of the consequences of this result is that E_g, being constant, does not affect the shape of the modulus of $\mathscr{U}$ (equation (6.5)). However, the phase is still not known.

6.2.1. *Phase reconstruction for dominant structures*

Three methods have been used to compute the phase information: (*a*) three-point correlations; (*b*) compactness in physical space; and (*c*) a 'spectral continuity' description of the dominant structure in Fourier space. The first two approaches were used by Herzog (1986) and Moin & Moser (1989) respectively. The third one, which has been chosen for the present work, will be detailed below.

This technique, also used by Moin & Moser (1989), consists of considering that, for neighbouring wavenumbers, the Fourier transform of the characteristic structure evolves slightly. Considering the inhomogeneous direction (y) and a single homogeneous direction, for example (z), this hypothesis can be written for two contiguous wavenumbers k_{z_a} and k_{z_b}:

$$\frac{\int \widetilde{\mathscr{U}}_i(y;k_{z_a})\widetilde{\mathscr{U}}_i^*(y;k_{z_b})\,\mathrm{d}y}{(\boldsymbol{\lambda}^{(1)}(k_{z_a})\boldsymbol{\lambda}^{(1)}(k_{z_b}))^{1/2}} \simeq 1. \tag{6.7}$$

This method leads to the phase determination relative to an additive constant that can be determined (but not its sign) by considering that the characteristic structure has to be real (i.e. the phase should be zero when $k_z \to 0$). This method will be used in the following Section in order to get a description of the dominant mode in physical space.

6.3. *Application of the 'shot-noise' theory*

In the present study, the spectral continuity method is used to characterize the phase function Θ and to describe the dominant structure in physical space. This specific approach was selected by considering several points. Moin & Moser (1989) have shown that the different approaches (spectral continuity, compactness or three-point correlations) lead globally to the same 'picture' of the dominant structure. The spectral continuity does not involve any statistical model for the spectral representation of the distribution function g used to describe the three-point correlations. It uses fewer *a priori* symmetries of the flow field than the spatial compactness does. It is based on, in some sense, a physical concept from which the spectral description of the dominant structure has to be 'smooth'.

In order to solve this problem, equation (6.7) is generalized to two spectral directions k_x and k_z. For each pair of wavenumbers $\boldsymbol{K}$, the neighbouring wavenumbers $\boldsymbol{K}'$ lying in the range $[\boldsymbol{K} \pm \Delta\boldsymbol{K}]$, have to be such that the inner product

$$\sum_{i=1}^{3} \int \widetilde{\mathscr{U}}_i(y;\boldsymbol{K})\,\widetilde{\mathscr{U}}_i^*(y;\boldsymbol{K}')\,\mathrm{d}y$$

is as close as possible to the eigenvalues square root product: $(\boldsymbol{\lambda}^{(1)}(\boldsymbol{K})\boldsymbol{\lambda}^{(1)}(\boldsymbol{K}'))^{1/2}$.
This problem is solved by using the following iterative procedure:

(*a*) the candidate function $\mathscr{U}_i$ is chosen such that

$$\widetilde{\mathscr{U}}_i(y;\boldsymbol{K}) = \left[\boldsymbol{\lambda}^{(1)}(\boldsymbol{K})\right]^{1/2} \boldsymbol{\Phi}_i^{(1)}(y;\boldsymbol{K});$$

(*b*) the phase function is initialized to zero for wavenumbers $\boldsymbol{K} = 0$;

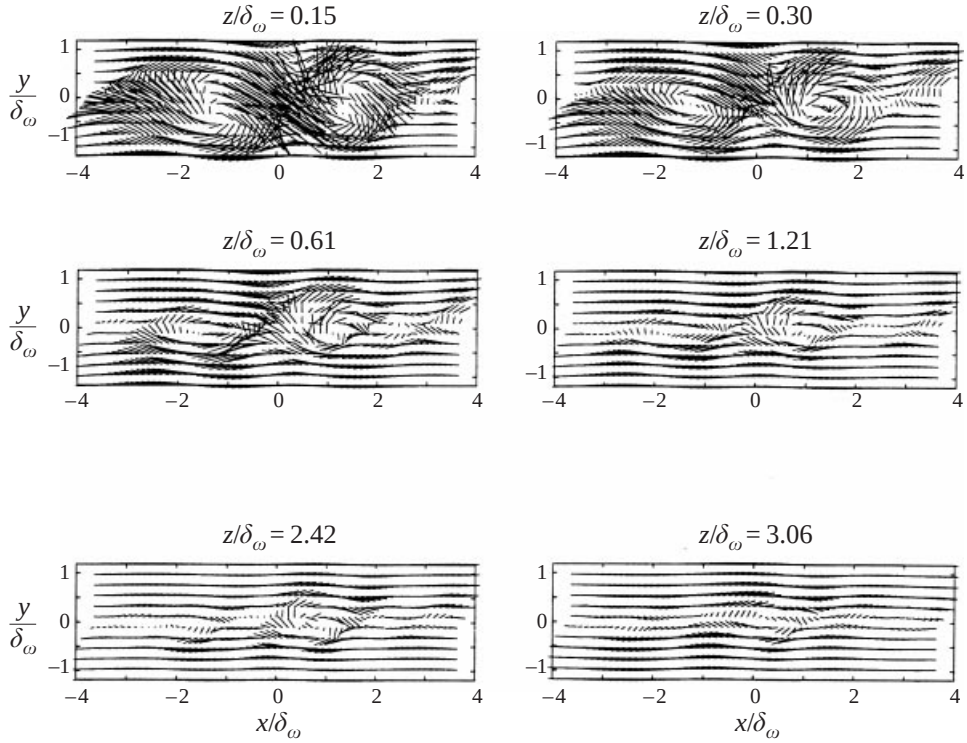

FIGURE 14. Velocity vector fields, of the dominant mode, viewed in (x, y)-planes for various spanwise locations and plotted in a framework following the flow using the convective velocity U_c.

(*c*) for each pair $\boldsymbol{K}$, one calculates the average over $(\pm\Delta\boldsymbol{K})$ of the scalar products:

$$\int_{-\Delta\boldsymbol{K}}^{+\Delta\boldsymbol{K}} \sum_{i=1}^{3} \int_{-L_y/2}^{+L_y/2} \widetilde{\mathscr{U}}_i(y;\boldsymbol{K})\,\widetilde{\mathscr{U}}_i^{*}(y;\boldsymbol{K}+\delta\boldsymbol{K})\mathrm{d}y\,\mathrm{d}\delta\boldsymbol{K},$$

which has a phase $\Theta_s(\boldsymbol{K})$;

(*d*) the phase is corrected with $-\Theta_s(\boldsymbol{K})$;

(*e*) return to point (c) until convergence is obtained.

A 'static image' of the dominant structure obtained by this method is given in figures 14 and 15. The wavenumber range $\Delta\boldsymbol{K}$ used for this reconstruction was $\Delta k_x\delta_\omega = \Delta k_z\delta_\omega = 0.1$. The velocity field obtained is periodic in the z- and x-directions. In the following a window is used which is centred at $x = z = 0$. The windows limits are $\pm 3.6\,\delta_\omega$, $\pm 1.1\,\delta_\omega$ and $\pm 3.2\,\delta_\omega$ in the x-, y- and z-directions, respectively.

The symmetries that the eigenvectors exhibit are imposed onto the components of the 'characteristic' velocity field: $\mathscr{U}_1$ and $\mathscr{U}_2$ are even while $\mathscr{U}_3$ is an odd function of z.

The resulting velocity field is shown in figure 14 for several (x, y)-planes and in figure 15 for (z, y)-planes, in a framework moving at the convective velocity U_c. The global convective velocity is used in order to emphasize the large-scale motion related to the spanwise vorticity ω_z. The quantities plotted are $\overline{U}^{(1)} - U_c + \mathscr{U}_1(x, y, z)$, $\mathscr{U}_2(x, y, z)$ and $\mathscr{U}_3(x, y, z)$. The term $\overline{U}^{(1)} - U_c$, added to the longitudinal component, is representative of the mean longitudinal velocity gradient. Since we are considering

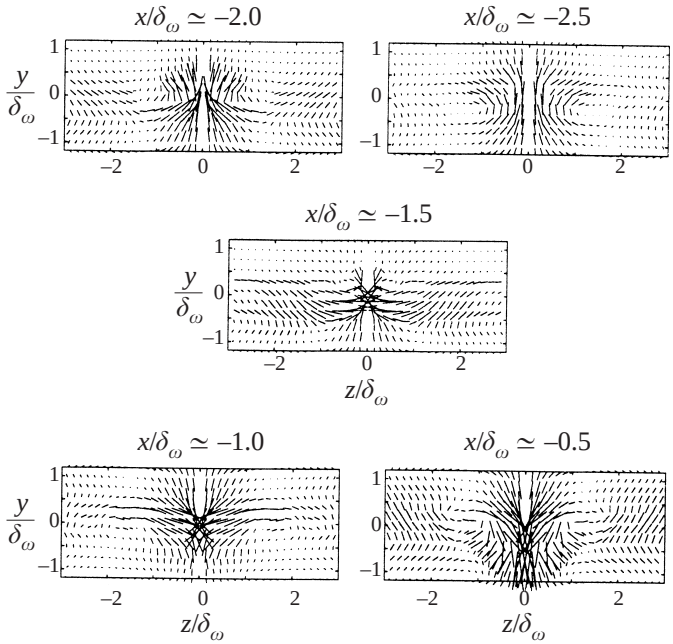

FIGURE 15. Velocity vector fields of the dominant mode, viewed in (z, y)-planes for various streamwise locations.

only the first POD mode, the directly measured mean velocity gradient cannot be used to translate the effects of the vorticity induced by the mean shear on the flow field. This problem is of the same nature as the one encountered in the dynamical systems approach when dealing with the relationship between the averaged field and the POD modes retained in the Galerkin projection (see Aubry *et al*. 1988). In order to scale the mean velocity gradient to the first POD mode, a mean velocity profile $\overline{U}^{(1)}$ is calculated from this mode by considering a Boussinesq approximation (Boussinesq 1877) and integrating the $\langle u'v'\rangle^{(1)}(y)$ profile in the y-direction. Here $\langle u'v'\rangle^{(1)}(y)$ is the contribution of mode (1) to the Reynolds stress $\langle u'v'\rangle$. This procedure leads to an 'equivalent' difference of velocity $\Delta U^{(1)}$ of about 12.3 m s^{-1}, somewhat smaller than the one directly measured (ΔU=17.6 m s^{-1}).

The dominant organization obtained is shown in figure 14 and corresponds to two large eddies, located at $x = \pm 1.5\delta_\omega$ and therefore separated about $3\delta_\omega$ in the streamwise direction. In fact, the centre of the domain is located on a saddle point. This result is consistent with the fact that the POD selects the more 'energetic' structure. The dominant mode is then centred where the turbulence production is maximum, i.e. the braid (Hussain 1986). Note that when z increases, the magnitude of the velocity decreases. This is due to the decrease of the spanwise correlation for large spanwise separations. A similar feature, although less pronounced, is observed if one considers the largest $|x|$ location. Another interesting feature can be found on this figure, when considering planes located at a large distance from $z = 0$. The centre of the eddies is gradually displaced upstream. For $z \simeq 3\delta_\omega$, the dominant eddy is centred on $x = 0$. This indicates that the dominant organization is modulated in the spanwise direction, the axis of the spanwise aligned vortex being tilted in the (x, z)-plane.

Selected slices of the velocity field in planes normal to the streamwise direction

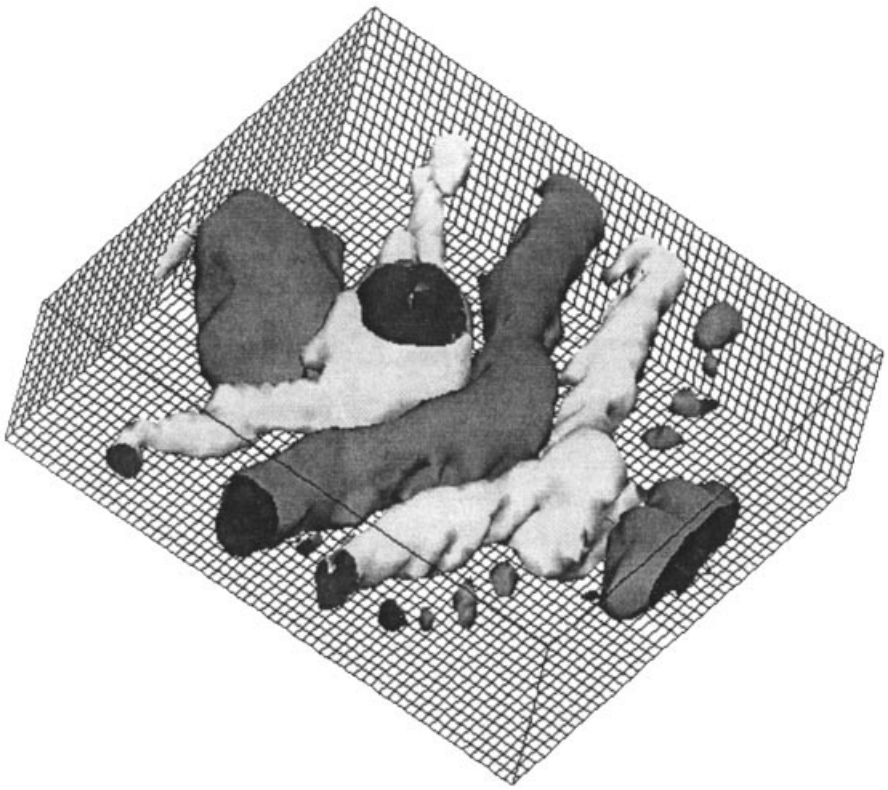

FIGURE 16. Iso-surfaces of velocity $\mathscr{U}_2$ component of the dominant mode – dark grey, $\mathscr{U}_2$=0.02ΔU – light grey, $\mathscr{U}_2$=-0.02ΔU. Size of the box L_x=7.3δ_ω, L_y=2.4δ_ω and L_z=6.4δ_ω.

are plotted on figure 15. By considering the $\mathscr{U}_3$ and $\mathscr{U}_2$ velocity components of the dominant structure in (z, y) cross-sections, an illustration of the streamwise vorticity ω_x is obtained. We focus here on the left-hand-side structure ($x < 0$) appearing in figure 14. Note that symmetrical trends are found if x-positive planes are considered. Near $z = 0$, two dominant motions can be seen: when upstream sections are considered ($x < x_c$) the flow goes upward, while at downstream sections ($x > x_c$) a downward fluid motion is observed. These motions are associated with counter-rotating streamwise vortices separated by from about $3.2\delta_\omega$ at $|x - x_c| \simeq \delta_\omega$ to about $2\delta_\omega$ at $|x - x_c| \simeq 0.5\delta_\omega$. Near the dominant structure core (i.e. $x \simeq -1.5\delta_\omega$) the global flux in the (z, y)-plane is nearly zero and, at this location, the spanwise wavelength is about $6\delta_\omega$. Note that the symmetries applied in the z-direction impose the appearance of this kind of organization.

The modulation of the spatial organization of the dominant mode can be clearly seen in figure 16 where a perspective view of iso-surfaces of the $\mathscr{U}_2$ velocity component are plotted. This velocity component (corresponding to the one normal to the splitter plate) is indicative of the global organization of the quasi-two-dimensional dominant structure. This kind of plot is preferred here to more conventional vorticity iso-surface plots, because of the correlation damping which results in the attenuation of the velocity levels with the distance from the centre of the box and hence no significant vortices would be found. Nevertheless, from this plot it appears clear that this dominant mode is strongly distorted. The resulting organization is in agreement

with the well-established notion of lambda-shaped organization of the mixing layer (see Nygaard & Glezer 1991 and Lesieur 1993).

7. Conclusions

The large-scale structures in a plane turbulent mixing layer have been studied through the use of correlations and the POD. The correlation tensor has been calculated from data collected with two rakes of cross-wires lying perpendicular to the splitter plate. Two separate experiments were performed to acquire the necessary data and the missing information was filled in by using the continuity relationship. The POD has been applied twice: first, to only the u- and v-components of the correlation tensor and, secondly, to the full correlation tensor, i.e. u, v and w information.

The auto-spectra exhibit characteristics consistent with the known phenomena for this flow field. In the outer part of the mixing layer, the uu-, vv- and ww-components all have a broad-band peak at the characteristic wavelength associated with the large-scale spanwise organization $k_1\delta_\omega \simeq 0.3$, while having very little energy past our measured third spanwise wavenumber. The vv and ww spectra also exhibited this behaviour near the centre of the mixing layer; however, the ww spectrum is broader band in k_3. Near the centre of the mixing layer the uu spectra exhibited significantly different behaviour from the other spectra, with the streamwise wavenumber peaking at approximately half the value was observed on the edge.

The solution of the eigenvalue problem has shown the rapid convergence of the POD modes. The first mode contained approximately 49% of the turbulent kinetic energy while 99% was captured with approximately seven modes. The eigenvalue spectra appeared to be the combination of the individual velocity auto-spectra with the broad-band peak at $k_1\delta_\omega \simeq 0.3$ along with the information in the low spanwise/streamwise wavenumber corner which is representative of the centre of the mixing layer. The addition of the w information only seemed to affect this area, which is representative of the secondary structure in the mixing layer. This seems consistent with geometric arguments about the flow structure in the mixing layer, in which one would not expect the spanwise structures to contain much kinetic energy that can be attributed to the w-component. However, near the centre of the mixing layer a significant amount of the energy can be attributed to the w-component. The eigenfunctions for the first mode have also been shown to contain the essential physics of the flow.

Applying the shot-noise theory to the first POD mode allowed the representation of a static description of the 'dominant mode' in physical space. The phase indetermination in the homogeneous directions was solved by considering the spectral continuity concept for the candidate structure. The 'structure' obtained corresponds to two quasi-two-dimensional vortices, whose axes are globally spanwise orientated, separated by about three times the vorticity thickness in the streamwise direction. Remarkably, with this approach, the dominant mode is centred on a zone located between two large-scale quasi-two-dimensional structures. This result is consistent with the nature of the POD which provides an optimal description in terms of energy: the resulting structure therefore points to a 'energetical area,' the saddle point, where most of turbulent energy production occurs. These vortices are found to be distorted in the spanwise direction. Contra-rotative streamwise-aligned vortices are also contained in this first POD mode, whose spanwise distance varies from one and a half to three times the vorticity thickness, depending on the location considered within the structure. The results are in agreement with the network or lambda-shaped organization notions of the turbulent mixing layer.

The rapid convergence of the POD modes, along with capturing of the essential flow physics in the first mode, suggests that the development of a low-dimensional dynamical systems model would be fruitful. Such a model has been developed and is the subject of Part 2.

This work was completed with the support of the French Ministery of Defense under the Grants DRET/DGA 90-171 and DRET/DGA 93.2549.A and a NSF/CNRS travel grant through the international program. Partial support for L. U. was provided by the French Ministery of Foreign Office under the Chateaubriand program. None of the experiments involved would have been posible without the contribution of H. Garem who designed the experimental arrangement.

REFERENCES

Arndt, R. E. A., Long, D. F. & Glauser, M. N. 1997 The proper orthogonal decomposition of the pressure fluctuation surrounding a turbulent jet. *J. Fluid Mech.* **340**, 1–33.

Aubry, N., Holmes, P., Lumley, J. L. & Stone, E. 1988 The dynamics of coherent structures in the wall region of a turbulent boundary layer. *J. Fluid Mech.* **192**, 115–173.

Bakewell, P. & Lumley, J. L. 1967 Viscous sublayer and adjacent wall region in turbulent pipe flow. *Phys. Fluids* **10**, 1880–1889.

Bell, J. H. & Mehta R. D. 1992 Measurements of streamwise vortical structures in a plane mixing layer. *J. Fluid Mech.* **239**, 213–248.

Bellin, S. 1991 Etude expérimentale des structures cohérentes d'une couche de mélange plane turbulente de fluide incompressible. PhD Thesis, University of Poitiers, France.

Berkooz, G. 1991 Turbulence, coherent structures and low dimensional models. PhD Thesis, Cornell University.

Berkooz, G., Holmes, P. & Lumley, J. L. 1993 The proper orthogonal decomposition in the analysis of turbulent flows. *Ann. Rev. Fluid Mech.* **25**, 539–575.

Bernal, L. P. & Rohko A. 1986 Streamwise vortex structure in plane mixing layers. *J. Fluid Mech.* **170**, 499–525.

Bonnet, J. P., Cole, D. R., Delville, J. Glauser, M. N. & Ukeiley, L. S. 1994 Stochastic estimation and proper orthogonal decomposition: complementary techniques for identifying structure. *Exps. Fluids* **17**, 307–314.

Boussinesq, T. V. 1877 Théorie de l'écoulement tourbillonnant, *Mém. Pré. par div. Sav. Paris*, **23**.

Breidenthal, R. E. 1978 A chemically reacting turbulent shear flow. PhD Thesis, California Institute of Technology.

Browand, F. K. 1986 The structure of the turbulent mixing layer. *Physica* D **18**, 135–148.

Browand, F. K. & Ho, C. M. 1983 The mixing layer – an example of quasi two-dimensional turbulence. *J. Méc. Théor. Appl.* Special Issue, 99.

Brown, G. L. & Roshko, A. 1974 On density effects and large scale structures in turbulent mixing layers. *J. Fluid Mech.* **64**, 775–816.

Bruun, H. H. 1995 *Hot-Wire Anemometry – Principles and Signal Analysis*. Oxford University Press.

Chambers, D. H., Adrian, R. J., Moin, P., Stewart, D. S. & Sung, H. J. 1988 Karhunen-Loeve expansion of Burgers' model of turbulence. *Phys. Fluids* **31**, 2573–2582.

Cordier, L., Delville, J. & Tenaud, C. 1997 Low dimensional description of large scale structures dynamics in a plane turbulent mixing layer. *Eleventh Symp. on Turbulent Shear Flows, Grenoble, France.*

Delville, J. 1994 Characterization of the organization in shear layers via the proper orthogonal decomposition. *Appl. Sci. Res.* **53**, 263–281.

Delville, J. 1995 La décomposition orthogonale aux valeurs propres et l'analyse de l'organisation tridimensionelle des écoulements turbulents cisaillés libres. PhD Thesis, University of Poitiers.

Delville, J., Bellin, S. & Bonnet, J. P. 1989 Use of the proper orthogonal decomposition in a plane turbulent mixing layer. In *Turbulence and Coherent Structures* (ed. O. Métais & M. Lesieur), pp. 75–90. Kluwer.

Delville, J., Bellin, S., Garem, J. H. & Bonnet, J. P. 1988 Analysis of structures in a turbulent

plane mixing layer by use of a pseudo flow visualization method based hot-wire anemometry. In *Advances in Turbulence II* (ed. H. H. Fernholtz & H. E. Fielder). Springer.

Delville, J. & Ukeiley, L. 1993 Vectorial proper orthogonal decomposition, including spanwise dependency, in a plane fully turbulent mixing layer. *Ninth Symp. on Turbulent Shear Flows, Kyoto, Japan.*

Delville, J., Vincendeau, E., Ukeiley, L., Garem, J. H. & Bonnet J. P. 1993 Etude expérimentale de la structure d'une couche de mélange plane turbulente en fluide incompressible. Application de la décomposition orthogonale aux valeurs propres. *Convention DRET* 90-171 Rapport Final.

Faghani, D. 1997 Etude des structures tourbillonnaires de la zone proche d'un jet plan: approche non stationnaire multidimensionnelle. PhD Thesis, Institut National Polytechnique de Toulouse, France.

George, W. K. 1988 Insight into the dynamics of coherent structures from a proper orthogonal decomposition. *Proc. Symp. on Near Wall Turbulence, Dubrovnik, Yugoslavia*, May 16–20.

Glauser, M. N. & George, W. K. 1987 An orthogonal decomposition of the axisymmetric jet mixing layer utilizing cross-wire measurements. *Sixth Symp. on Turbulent Shear Flows, Toulouse, France.*

Glauser, M. N. & George, W. K. 1992 Application of multipoint measurements for flow characterization. *Expl Thermal Fluid Sci.* **5**, 617–632.

Glauser, M. N., Leib, S. J. & George, W. K. 1987 Coherent structures in the axisymmetric jet mixing layer. In *Turbulent Shear Flows 5* (ed. F. Durst *et al*.), p. 134. Springer.

Glezer, A., Kadioglu, A. J. & Pearlstein, A. J. 1989 Development of an extended proper orthogonal decomposition and its application to a time periodically forced plane mixing layer. *Phys. Fluids* A **1**, 1363–1373.

Herzog, S. 1986 The large scale structure in the near-wall of turbulent pipe flow. PhD Thesis, Cornell University.

Ho, C. M. & Huerre, P. 1984 Perturbed free shear layers. *Ann. Rev. Fluid Mech.* **16**, 365–424.

Holmes, P., Lumley, J. L. & Berkooz, G. 1996 *Turbulence, Coherent Structures, Dynamical Systems and Symmetry*. Cambridge University Press.

Hussain, A. K. M. F. 1986 Coherent structures and turbulence. *J. Fluid Mech.* **173**, 303–356.

Konrad, J. H. 1976 An experimental investigation of mixing in two-dimensional turbulent shear flows with applications to diffusion-limited chemical reaction. PhD Thesis, California Institute of Technology.

Lasheras, J. C. & Choi, H. 1988 Three-dimensional instability of a plane free shear layer: an experimental study of the formation and evolution of streamwise vortices. *J. Fluid Mech.* **189**, 53–86.

Lasheras, J. C. & Meiburg, E. 1990 Three-dimensional vorticity modes in the wake of a flat plate. *Phys. Fluids* **2**, 371–380.

Leboeuf, R. & Mehta, R. 1993 Streamwise vortex meander in a plane mixing layer. *Phys. Fluids* A **5**, 1983–1991.

Leboeuf, R. & Mehta, R. 1995 On using Taylor's hypothesis for three-dimensional mixing layers. *Phys. Fluids* **7**, 1516–1518.

Leib, S. J., Glauser, M. N. & George, W. K. 1984 An application of Lumley's orthogonal decomposition to the axisymmetric jet mixing layer. *Proc. 9th Rolla Symp.* (directed by X. B. Reed, G. K. Patterson & J. L. Zakin). University of Missouri, Rolla.

Lesieur, M. 1993 Understanding coherent vortices through computational fluid dynamics. *Theor. Comput. Fluid Dyn.* **5**, 177-193.

Liu, J. T. C. 1989 Coherent Structures in transitional and turbulent free shear flows. *Ann. Rev. Fluid Mech.* **21**, 285–315.

Liu, Z. C., Adrian, R. J. & Hanratty, T. J. 1995 A study of turbulent channel flow with 2-D proper orthogonal decomposition. *Bull. Am. Phys. Soc.* **40**, 2014.

Loeve, M. 1955 *Probability Theory*. Van Nostrand.

Lumley, J. L. 1967 The structure of inhomogeneous turbulent flows. In *Atmospheric Turbulence and Radio Wave Propagation* (ed. A. M. Yaglom & V. I. Tatarsky), pp. 166–178. Nauka, Moscow.

Lumley, J. L. 1981 Coherent structures in turbulence. In *Transition and Turbulence* (ed. R. E. Meyer), pp. 215–242. Academic Press.

Manhart, M. & Wengle, H. 1993 A spatiotemporal decomposition of a fully inhomogeneous turbulent flow field. *Theor. Comput. Fluid Dyn.* **5**, 223–242.

Meiburg, E. & Lasheras, J. C. 1988 Experimental and numerical investigation of the three-dimensional transition in plane wakes. *J. Fluid Mech.* **190**, 1–37.

Metcalfe, R. W., Orszag, S. A., Brachet, M. E., Menon, M. & Riley, J. J. 1987 Secondary instability of a temporally growing mixing layer. *J. Fluid Mech.* **184**, 207–243.

Moin, P. 1984 Probing turbulence via large eddy simulation. *AIAA Paper* 84-0174.

Moin, P. & Moser, R. D. 1989 Characteristic-eddy decomposition of turbulence in a channel. *J. Fluid Mech.* **200**, 471–509.

Moser, R. D. & Rogers, M. M. 1992 Coherent structure in a simulated turbulent mixing layer. In *Eddy Structure Identification in Free Turbulent Shear Flows* (ed. J. P. Bonnet & M. N. Glauser). Kluwer.

Nygaard, K. J. & Glezer, A. 1991 Evolution of streamwise vortices and generation of small-scale motion in a plane mixing layer. *J. Fluid Mech.* **231**, 257–301.

Payne, F. R. 1966 Large eddy structure of a turbulent wake. PhD Thesis, Pennsylvania State University.

Pierrehumbert, R. T. & Widnall, S. E. 1982 The two- and three-dimensional instabilities of a spatially periodic shear layer. *J. Fluid Mech.* **114**, 59–82.

Rajaee, M., Karlsson, S. & Sirovich, L. 1994 Low-dimensional description of free-shear-flow coherent structures and their dynamical behaviour. *J. Fluid Mech.* **258**, 1–29.

Rempfer, D. & Fasel, H. F. 1994 Evolution of three-dimensional coherent structures in a flat-plate boundary layer. *J. Fluid Mech.* **260**, 351–375.

Rice, S. O. 1954 Mathematical analysis of random noise. *Bell System Tech. J.* 282–332.

Sirovich, L. 1987 Turbulence and the dynamics of coherent structures, Part 1: Coherent structures. *Q. Appl. Maths* **XLV**, 561–571.

Ukeiley, L. S., Cole, D. R. & Glauser, M. N. 1993 An examination of the axisymmetric jet mixing layer using coherent structure detection techniques. In *Eddy Structure Identification in Free Turbulent Shear Flows* (ed. J. P. Bonnet & M. N. Glauser). Kluwer.

Ukeiley, L., Cordier, L., Delville, J., Glauser, M. & Bonnet, J. P. 1999 Examination of large-scale structures in a turbulent plane mixing layer. Part 2. Dynamical systems model. *J. Fluid Mech.* (submitted).

Ukeiley, L., Glauser, M. & Wick, D. 1993 Downstream evolution of proper orthogonal decomposition eigenfunctions in a lobed mixer. *AIAA J.* **31**, 1392–1397.

Ukeiley, L., Varghese, M., Glauser, M. & Valentine, D. 1992 Multifractal analysis of a lobed mixer flowfield utilizing the proper orthogonal decomposition. *AIAA J.* **30**, 1260–1267.

Zaman, K. M. B. Q. & Hussain, A. K. M. F. 1981 Taylor hypothesis and large-scale coherent structures. *J. Fluid Mech.* **112**, 379–396.

Zheng, X. & Glauser M. 1991 A low dimensional dynamical systems description of coherent structures in the axisymmetric jet mixing layer. *Rep.* MAE-247. Clarkson University.